Actin- and microtubule-based motors contribute to clathrin-independent endocytosis in yeast

Thaddeus K. Woodard[a], Daniel J. Rioux[b,c], and Derek C. Prosser [b,*]
[a]Department of Biology, The Johns Hopkins University, Baltimore, MD 21218; [b]Department of Biology, and [c]Life Sciences, Virginia Commonwealth University, Richmond, VA 23284

ABSTRACT Most eukaryotic cells utilize clathrin-mediated endocytosis as well as multiple clathrin-independent pathways to internalize proteins and membranes. Although clathrin-mediated endocytosis has been studied extensively and many machinery proteins have been identified, clathrin-independent pathways remain poorly characterized by comparison. We previously identified the first known yeast clathrin-independent endocytic pathway, which relies on the actin-modulating GTPase Rho1, the formin Bni1 and unbranched actin filaments, but does not require the clathrin coat or core clathrin machinery proteins. In this study, we sought to better understand clathrin-independent endocytosis in yeast by exploring the role of myosins as actin-based motors, because actin is required for endocytosis in yeast. We find that Myo2, which transports secretory vesicles, organelles and microtubules along actin cables to sites of polarized growth, participates in clathrin-independent endocytosis. Unexpectedly, the ability of Myo2 to transport microtubule plus ends to the cell cortex appears to be required for its role in clathrin-independent endocytosis. In addition, dynein, dynactin, and proteins involved in cortical microtubule capture are also required. Thus, our results suggest that interplay between actin and microtubules contributes to clathrin-independent internalization in yeast.

SIGNIFICANCE STATEMENT

- Eukaryotic cells utilize endocytosis to internalize material. While clathrin-mediated endocytosis is the primary route, multiple clathrin-independent pathways have been observed but remain poorly understood. Previous studies identified a yeast clathrin-independent pathway that requires the Rho1 GTPase, the formin Bni1, and actin.

- Here, the authors use genetics and quantitative microscopy to expand the set of proteins involved, implicating myosin, microtubules, and microtubule-based motors.

- These findings provide new information about the set of proteins needed for clathrin-independent endocytosis. Many of the genes involved in the yeast pathway are conserved through evolution, and may provide important context for endocytosis in other cell types.

INTRODUCTION

In eukaryotic cells, the plasma membrane (PM) plays important roles in regulation of signal transduction, communication with the extracellular environment, and nutrient uptake. Maintenance of PM composition and function relies on a balance between exocytosis for delivery of membrane and proteins and on endocytosis for their internalization and removal from the cell surface. Exocytic- and endocytic transport allow the cell to control the complement of proteins at the PM in order to amplify or attenuate responses to external cues, and permit selective uptake of nutrients by regulating surface availability of transporters. Additionally, endocytosis plays

important quality control functions in mediating removal of damaged proteins through internalization and targeting to the lysosome for degradation.

Endocytic mechanisms have been studied extensively for over 60 y, where electron microscopy studies observed "bristle-coated" structures that were later identified as clathrin-coated pits and vesicles (Roth and Porter, 1964; Kanaseki and Kadota, 1969; Pearse, 1975). Subsequent studies have characterized clathrin-mediated endocytosis (CME) as the predominant pathway for internalization in most eukaryotic cells (Kaksonen and Roux, 2018). CME is highly conserved from yeast to human, and involves the action of more than 40 distinct proteins that arrive in a highly ordered sequence of events in order to select and concentrate cargo at sites of vesicle formation (Kaksonen et al., 2003, 2005; Taylor et al., 2011). These proteins act in modules that correspond to discrete stages of clathrin-coated vesicle (CCV) formation, beginning with an initiation phase in which adaptor proteins bind to endocytic cargos at the PM as well as the assembling clathrin coat, effectively concentrating the cargo at a site of CCV formation (Howard et al., 2002; Newpher et al., 2005; Maldonado-Báez et al., 2008; Reider et al., 2009; Reider and Wendland, 2011). As the clathrin-coated site matures, endocytic accessory and scaffolding proteins facilitate additional clathrin assembly, and recruit proteins involved in later stages of vesicle formation, including actin-nucleating proteins in yeast required for the force generation needed for membrane invagination (Kaksonen et al., 2003, 2005; Sun et al., 2006). In the late stages of CME, scission effectors such as dynamin and amphiphysins assist with membrane constriction at the neck of the budding vesicle, leading to separation of the CCV from the cell surface (Bliek et al., 1993; Damke et al., 1994; Kaksonen et al., 2005). Finally, uncoating of the CCV permits recycling of endocytic machinery proteins and fusion of the vesicle with downstream compartments (Ungewickell et al., 1995). Studies have shown that the modular nature of CME is well conserved, and genetic or pharmacological perturbation of any stage in the process can reduce the efficiency of cargo internalization (Goode et al., 2015; Kaksonen and Roux, 2018).

Early studies of endocytosis also observed vesicle formation in the absence of a bristle coat (Anderson and Batten, 1983; Morris and Saelinger, 1983), suggesting that multiple mechanisms for internalization likely existed. Indeed, numerous clathrin-independent endocytic (CIE) pathways have been identified across eukaryotes. These include a variety of mechanistically distinct routes of internalization. For example, CIE encompasses phagocytic and macropinocytic pathways that rely on membrane protrusion or ruffling, lipid (typically cholesterol)-enriched membrane microdomains such as caveolae and clathrin-independent carriers and GPI-enriched endocytic compartments (CLIC; GEEC), and actin-dependent pathways relying on Arf- and Rho-family small GTPases (Radhakrishna et al., 1996; Lamaze et al., 2001; Sabharanjak et al., 2002; Sharma et al., 2002; Howes et al., 2010; Mayor et al., 2014). In addition, recent studies have demonstrated that ultrafast endocytosis at synaptic terminals is clathrin-independent, and fast endophilin-mediated endocytosis (FEME) is a distinct CIE pathway that relies on Endophilin A1, dynein, and microtubules for internalization of PM proteins (Watanabe et al., 2013a, b; Boucrot et al., 2015; Casamento and Boucrot, 2020). Despite the variety of CIE pathways that have been documented, our current understanding of the molecular mechanisms governing any CIE pathway is poor in comparison to that of CME. Reasons for this disparity may include the comparative lack of cargos that utilize CIE pathways for entry, and a lack of genetically tractable model systems for studies of CIE.

We previously identified the first-known *Saccharomyces cerevisiae* CIE pathway using a mutant strain lacking four monomeric clathrin-binding adaptor proteins: the epsins Ent1 and Ent2, and the AP180/PICALM homologues Yap1801 and Yap1802 (Prosser et al., 2011). Yeast lacking these adaptors (*ent1Δ ent2Δ yap1801Δ yap1802Δ*, also known as 4Δ) have defective CME as seen by retention of endocytic cargos at the PM, while any one full-length adaptor is sufficient for endocytosis (Maldonado-Báez et al., 2008). Although *ENT1* and *ENT2* constitute an essential gene pair, expression of the phosphatidylinositol (4,5)-bisphosphate (PI[4,5]P$_2$)-binding epsin N-terminal homology (ENTH domain) of either gene is sufficient for viability but not for their role in CME (Wendland et al., 1999; Aguilar et al., 2006; Maldonado-Báez et al., 2008). Thus, 4Δ+ENTH1 cells expressing the ENTH domain of Ent1 have been a useful model for studying deficits in CME (Maldonado-Báez et al., 2008; Prosser et al., 2011). Using this strain to identify genes whose overexpression restored endocytic cargo internalization, we found that high-copy expression of the cell wall stress sensor *MID2*, the Rho1 guanine nucleotide exchange factor *ROM1* and the actin-modulating small GTPase *RHO1* all enhanced internalization of multiple endocytic cargos, and that their function did not require clathrin or the major CME machinery proteins (Prosser et al., 2011; Prosser and Wendland, 2012). The budding yeast CIE pathway additionally requires the formin Bni1, which generates unbranched actin filaments independent of Arp2/3, proteins in the polarisome complex which recruits and activates Bni1 at sites of polarized growth, and proteins that stabilize unbranched actin filaments such as the tropomyosins Tpm1 and Tpm2. Further studies identified α-arrestins as cargo-selective proteins that participate in CIE through mechanisms that are distinct from their established roles in CME, as well as a dual role for the early acting CME protein Syp1, suggesting that some proteins may contribute to multiple endocytic pathways (Prosser et al., 2015; Apel et al., 2017).

Although yeast were thought to rely solely upon CME before our identification of the Rho1-dependent CIE pathway, other studies have also suggested that yeast do not strictly require CME for cargo internalization. For example, *Candida albicans* can perform endocytosis in the absence of functional clathrin and Arp2/3 (Epp et al., 2010, 2013), while endocytosis at the cylindrical sides of cells in the fission yeast *Schizosaccharomyces pombe* appears to depend on the formin For3 (Gachet and Hyams, 2005). Overall, our mechanistic understanding of CIE pathways in yeast, and indeed in any eukaryotic-cell type, lags considerably behind that of CME due at least in part to a lack of tools to characterize these pathways.

In this study, we extend our earlier findings by expanding the set of proteins required for CIE in yeast. Because all endocytosis in yeast critically depends on actin polymerization, we specifically focused on roles for myosins as actin-based motors and on myosin-interacting proteins. We find that Myo2, which transports organelles and other cellular structures along actin cables to sites of polarized growth, is required for CIE. Unexpectedly, Myo2-dependent transport of microtubule plus ends, as well as dynein, dynactin, and proteins involved in cortical microtubule capture participate in CIE, while transport of other structures is dispensable. Thus, interplay between actin and microtubule cytoskeletons may play important roles in yeast CIE.

RESULTS

The type V myosin Myo2 is required for clathrin-independent endocytosis

Our previous studies of CIE demonstrated a requirement for the formin Bni1, which localizes mainly to the bud tip and bud neck,

where it promotes actin elongation at the barbed end of unbranched filaments (Evangelista *et al.*, 2001; Pruyne *et al.*, 2002; Sagot *et al.*, 2002; Prosser *et al.*, 2011). Additionally, we found that the tropomyosin Tpm1, which stabilizes unbranched actin filaments, was necessary for CIE. These filaments are bundled into actin cables that serve as tracks for myosin-dependent delivery of material to sites of polarized growth (Pruyne *et al.*, 1998). Our initial findings underscored the role of actin in CIE, and prompted us to examine the contribution of myosins as actin-based motors. Budding yeast possess five myosins: the type I myosins Myo3 and Myo5 are involved in CME and act at cortical actin patches, the type II myosin Myo1 is involved in constriction of the cytokinetic ring at the bud neck, and the type V myosins Myo2 and Myo4 transport proteins, vesicles, organelles, and mRNA along actin cables (Watts *et al.*, 1987; Bobola *et al.*, 1996; Geli and Riezman, 1996; Pruyne *et al.*, 2004). Of these, Myo2 appears to play the most prominent role in transport along unbranched actin cables; thus, we focused on this protein as a candidate motor involved in CIE.

Myo2 is an essential gene, and thus cannot be deleted (Johnston *et al.*, 1991). Instead, we generated *myo2* mutants with reduced processivity (Schott *et al.*, 1999, 2002). The lever arms of Myo2 permit movement along actin filaments, and contain IQ repeats that can be truncated to generate motors that take shorter "steps." Using full-length (6IQ) or truncated (4IQ or 2IQ) mutants expressed as the sole source of Myo2 in wild-type (WT), 4Δ+Ent1 (with functional CME) and 4Δ+ENTH1 (with impaired CME) backgrounds, we examined localization of the pheromone receptor Ste3-GFP as an endocytic cargo. Ste3 is a seven-transmembrane receptor that is normally transported to the PM in haploid *MATα* cells, constitutively internalized via CME, and delivered to the vacuole for degradation (Davis *et al.*, 1993). Under conditions where CME is blocked, Ste3 is instead largely retained at the PM, with reduced transport to the vacuole (Maldonado-Báez *et al.*, 2008). We previously found that expression of *ROM1* from a high-copy plasmid promoted clathrin-independent internalization of Ste3-GFP in numerous CME-deficient mutants including 4Δ+ENTH1 (Prosser *et al.*, 2011); thus, we asked whether a reduction in Myo2 processivity would impair *ROM1*-dependent activation of CIE. In WT and 4Δ+Ent1 backgrounds transformed with empty vector, expression of Myo2^{6IQ} (WT control), Myo2^{4IQ}, or Myo2^{2IQ} resulted in Ste3-GFP localization primarily at the vacuole (Figure 1A). Thus, reduced Myo2 processivity does not appear to affect CME. In contrast, Ste3-GFP showed increased retention at the PM in 4Δ+ENTH1 cells transformed with empty vector and expressing full-length and truncated Myo2, consistent with defective endocytosis in 4Δ+ENTH1 cells. When these 4Δ+ENTH1 cells were instead transformed with high-copy *ROM1* to promote CIE, we found that Ste3-GFP internalization and transport to the vacuole was improved in cells expressing full-length Myo2^{6IQ}, but showed less or no improvement in cells expressing Myo2^{4IQ} or Myo2^{2IQ} compared with equivalent empty vector-transformed cells.

We previously developed a quantitative method for assessing endocytic capacity in live yeast cells by tagging the cytoplasmic tail of cargo proteins with supereliptic pHluorin, a pH-sensitive variant of GFP (Miesenböck *et al.*, 1998; Sankaranarayanan *et al.*, 2000; Prosser *et al.*, 2010, 2016). When the tail of the cargo is exposed to a neutral environment such as the cytoplasm, the pHluorin tag is brightly fluorescent. In contrast, fluorescence is quenched upon packaging of the tag into acidic environments, such as the intraluminal vesicles within multivesicular bodies or the vacuole lumen. Measurement of steady-state, whole-cell Ste3-pHluorin intensity can thus reveal changes in endocytic capacity in ways that are difficult to measure using equivalent strains expressing Ste3-GFP: cells that ef-

ficiently internalize Ste3-pHluorin and target it to the vacuole are dim, while cells with defective endocytosis retain the tagged protein at the PM and are comparatively bright (Prosser *et al.*, 2010, 2016). Using the same truncated Myo2 strains expressing genomically tagged Ste3-pHluorin instead of GFP, we were able to quantitatively assess the effect of reduced Myo2 processivity on CIE. As expected for cells with defective CME, Ste3-pHluorin intensity in empty vector-transformed 4Δ+ENTH1 cells expressing full-length Myo2^{6IQ} or truncated Myo2^{4IQ} or Myo2^{2IQ} was significantly brighter than in the equivalent WT and 4Δ+Ent1 backgrounds (Figure 1B–D). In Myo2^{6IQ}-expressing 4Δ+ENTH1 cells, transformation with high-copy *ROM1* partially restored Ste3-pHluorin internalization, as shown by a significant reduction in fluorescence intensity compared with the same cells with empty vector (Figure 1B). In contrast, high-copy *ROM1* failed to improve Ste3-pHluorin internalization in 4Δ+ENTH1 cells expressing Myo2^{4IQ} (Figure 1C) or Myo2^{2IQ} (Figure 1D), as these cells remained as bright as, or brighter than, equivalent empty vector-transformed cells. Taken together, these data suggest that Myo2 processivity is required for CIE in yeast.

To examine the potential contribution of other myosins to CIE, we generated single *myo1Δ* and *myo4Δ* deletions in WT, 4Δ+Ent1, and 4Δ+ENTH1 backgrounds expressing Ste3-GFP. Both *myo1Δ* and *myo4Δ* did not alter vacuolar Ste3-GFP localization in WT and 4Δ+Ent1 backgrounds transformed with empty vector, suggesting that neither gene is required for cargo internalization when CME is functional (Supplemental Figure S1, A and B). Whereas Ste3-GFP was partially retained at the PM in empty vector-transformed *myo1Δ* or *myo4Δ* 4Δ+ENTH1 cells, transformation with high-copy *ROM1* reduced cell surface retention and increased vacuole localization in both cases, suggesting that neither Myo1 nor Myo4 is required for CIE.

Because Myo3 and Myo5 play overlapping roles in force generation at cortical actin patches in yeast, deletion of both genes simultaneously is required to block CME (Geli and Riezman, 1996). Consistent with this finding, *myo3Δ myo5Δ* cells transformed with empty vector showed a severe retention of Ste3-GFP at the PM, with cargo fluorescence virtually undetectable in the vacuole (Supplemental Figure S1, C and D). This defect could be complemented by low-copy expression of *MYO5*, which restored vacuolar Ste3-GFP localization and reduced cell surface retention of the cargo. In contrast, high-copy *YAP1801*, which restored endocytosis in 4Δ+ENTH1 cells, had no effect on cargo internalization in *myo3Δ myo5Δ* (Prosser *et al.*, 2011). Although we predicted that high-copy *ROM1* would promote CIE in *myo3Δ myo5Δ* cells because these myosins are known to function in CME, we unexpectedly found that Ste3-GFP was strongly retained at the PM. However, close examination of these cells revealed dim vacuolar fluorescence with high-copy *ROM1*, but not in cells transformed with empty vector or *YAP1801* (Supplemental Figure 1, C and D). The limited ability of Rom1 to promote Ste3 internalization in *myo3Δ myo5Δ* cells might be explained by previous studies showing that actin cable morphology is severely altered in this strain (Goodson *et al.*, 1996; Anderson *et al.*, 1998). Indeed, phalloidin staining of *myo3Δ myo5Δ* cells with empty vector revealed numerous actin patches, but no obvious actin cable structures (Supplemental Figure 1E). While low-copy *MYO5* restored actin cables, they remained absent in cells with high-copy *YAP1801* or *ROM1*. Thus, while Myo3 and Myo5 may play direct roles in CIE, their role might instead be explained by an indirect effect on actin cable morphology because both proteins appear to localize exclusively to cortical actin patches that are known sites of CME, but which do not appear to be involved in CIE (Sun *et al.*, 2006; Barker *et al.*, 2007; Prosser *et al.*, 2011). Taken together, these data suggest
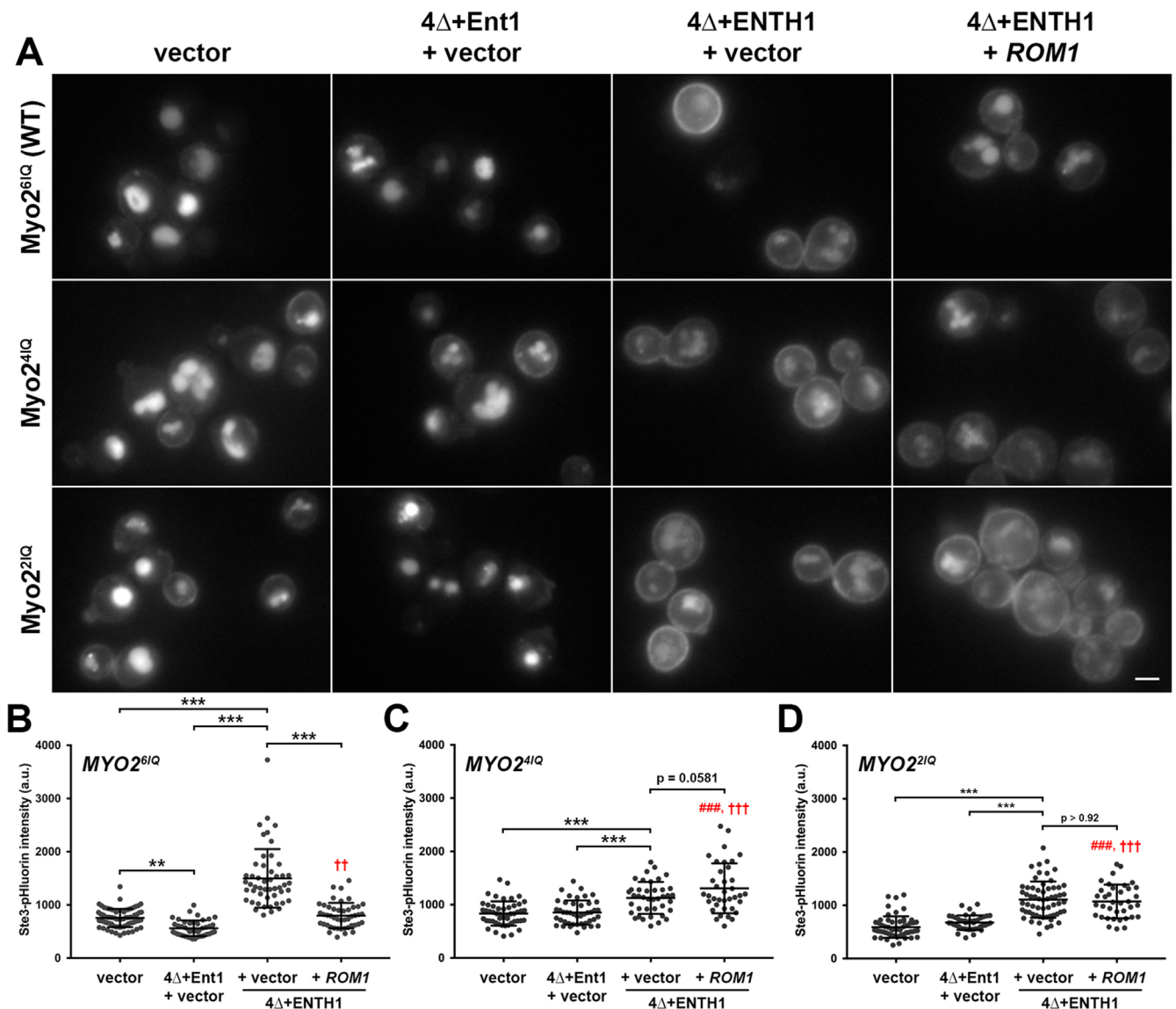
FIGURE 1: Effect of Myo2 IQ repeat truncation on clathrin-independent endocytosis. Full-length Myo2^{6IQ} or truncated Myo2^{4IQ} or Myo2^{2IQ} mutants expressed as the sole source of Myo2 in WT (vector), 4Δ+Ent1 and 4Δ+ENTH1 backgrounds were transformed with vector or high-copy *ROM1* as indicated. (A) Cells expressing Ste3-GFP from the endogenous locus were imaged by fluorescence microscopy. (B–D) Quantification of whole-cell fluorescence intensity in cells expressing Ste3-pHluorin transformed as in A. (B) Myo2^{6IQ} ($n = 73$, $n = 45$, $n = 50$ and $n = 46$, respectively). (C) Myo2^{4IQ} ($n = 50$, $n = 44$, $n = 40$ and $n = 37$, respectively). (D) Myo2^{2IQ} ($n = 58$, $n = 43$, $n = 60$ and $n = 37$, respectively). Mean ± SD; **$p < 0.01$, ***$p < 0.001$; ###$p < 0.001$ compared with WT; ††$p < 0.01$ and †††$p < 0.001$ compared with 4Δ+Ent1. Scale bar: 2 µm.

that Myo2 processivity contributes to CIE, while other myosins may play less prominent roles.

We previously found that the yeast CIE pathway can be activated in 4Δ+ENTH1 cells grown under high osmolarity conditions, without requiring *ROM1* overexpression (Prosser *et al.*, 2011). In these studies, 4Δ+ENTH1 cells showed improved Ste3-GFP internalization when grown on high-osmolarity medium (YPD medium + 1 M sorbitol) compared with low-osmolarity YPD medium. This effect required Bni1, Bud6 and Tpm1, which are all required for CIE but not for CME. To further test whether Myo2 contributes to CIE, we examined Ste3-GFP localization for Myo2^{6IQ}, Myo2^{4IQ}, and Myo2^{2IQ} strains in WT, 4Δ+Ent1 and 4Δ+ENTH1 backgrounds grown on YPD without or with 1 M sorbitol. When Myo2^{6IQ}, Myo2^{4IQ}, or Myo2^{2IQ} cells were

grown on YPD, Ste3-GFP localized primarily to the vacuole in all control (WT and 4Δ+Ent1) backgrounds with functional CME, and showed retention at the PM in all 4Δ+ENTH1 backgrounds as expected (Supplemental Figure S2). Similarly, all control (WT and 4Δ+Ent1) backgrounds showed prominent vacuolar Ste3-GFP when cells were grown on YPD + 1 M sorbitol. When we examined Ste3-GFP localization in Myo2^{6IQ}, Myo2^{4IQ}, and Myo2^{2IQ} 4Δ+ENTH1 cells, we found that Ste3-GFP internalization was partially improved in Myo2^{6IQ}, but not in Myo2^{4IQ} or Myo2^{2IQ} 4Δ+ENTH1 cells. These results are consistent with our observation that high-copy *ROM1* could not promote Ste3 internalization when Myo2 IQ repeats were truncated (Figure 1), and suggest that Myo2 contributes to CIE under a second condition that promotes the pathway.

Myo2-dependent transport of microtubules is required for CIE

Previous studies showed that Myo2 plays a critical role in mother-to-bud transport of secretory vesicles, mitochondria, vacuoles, peroxisomes, and microtubules (Pruyne *et al.*, 1998; Schott *et al.*, 1999; Beach *et al.*, 2000; Ishikawa *et al.*, 2003; Boldogh *et al.*, 2004; Fagarasanu *et al.*, 2005, 2009). To achieve this, the cargo-binding domain (CBD) of Myo2 interacts with organelle-specific adaptors that link each structure to the motor for transport (Pashkova *et al.*, 2006; Lipatova *et al.*, 2008; Fagarasanu *et al.*, 2009; Jin *et al.*, 2011; Eves *et al.*, 2012). Structure-function analysis of the CBD revealed unique surface patches that associate with Myo2 adaptors, and mutations within these patches result in selective loss of adaptor binding and organelle transport (Pashkova *et al.*, 2006; Eves *et al.*, 2012). To assess which functions are necessary for CIE, we expressed CBD mutants from the endogenous Myo2 locus as the sole source of Myo2 in WT, 4Δ+Ent1, and 4Δ+ENTH1 backgrounds. We focused on five point mutants, each defective in one transport function: 1) D1297N (loss of Vac17 binding and vacuole transport); 2) K1312A (loss of Mmr1 binding and mitochondrial transport); 3) K1408A (loss of Kar9 binding and microtubule plus-end transport); 4) Q1447R (deficient in binding the Rab GTPases Ypt31, Ypt32, Ypt11, and Sec4, reduction in secretory vesicle transport); 5) and E1484A (loss of Inp2 binding and peroxisome transport (Ishikawa *et al.*, 2003; Pashkova *et al.*, 2006; Lipatova *et al.*, 2008; Fagarasanu *et al.*, 2009; Eves *et al.*, 2012). All of these point mutants were previously shown to express at levels similar to WT Myo2 when expressed as the sole source of protein from low-copy plasmids in *myo2Δ* cells (Eves *et al.*, 2012). As seen in Figure 2A, expression of any of these mutants in WT or 4Δ+Ent1 cells transformed with empty vector did not alter vacuolar localization of Ste3-GFP compared with cells with WT Myo2, suggesting that none of these Myo2 functions impact CME. As expected for 4Δ+ENTH1 cells expressing Myo2 CBD mutants and transformed with empty vector, Ste3-GFP showed retention at the PM. Expression of high-copy *ROM1* improved Ste3-GFP internalization and vacuolar delivery in 4Δ+ENTH1 cells expressing WT Myo2 and all of the CBD mutants except for the microtubule transport-deficient mutant, Myo2^{K1408A}.
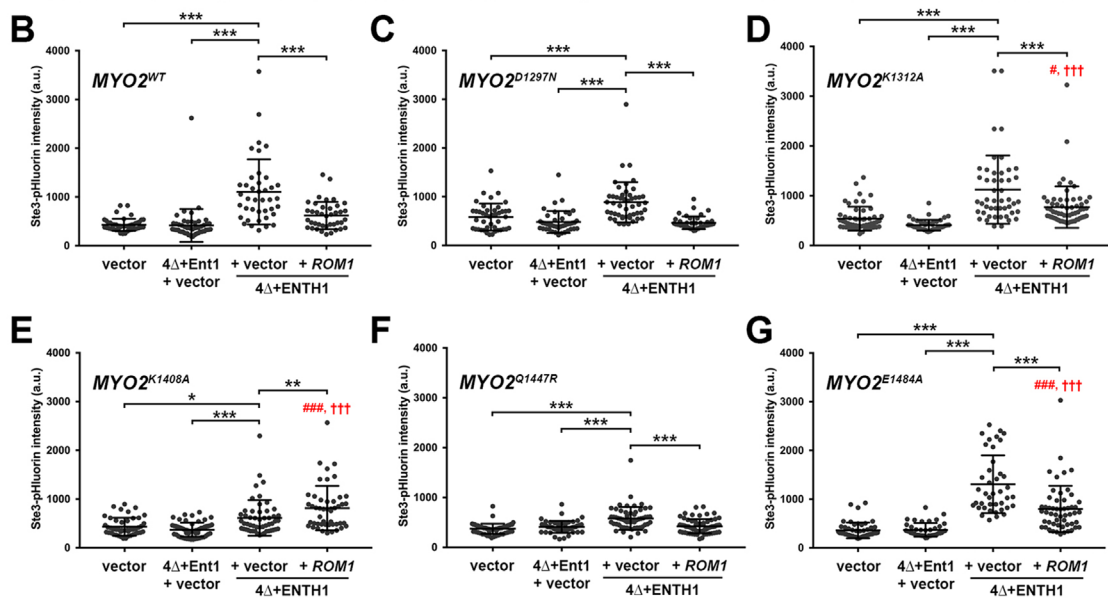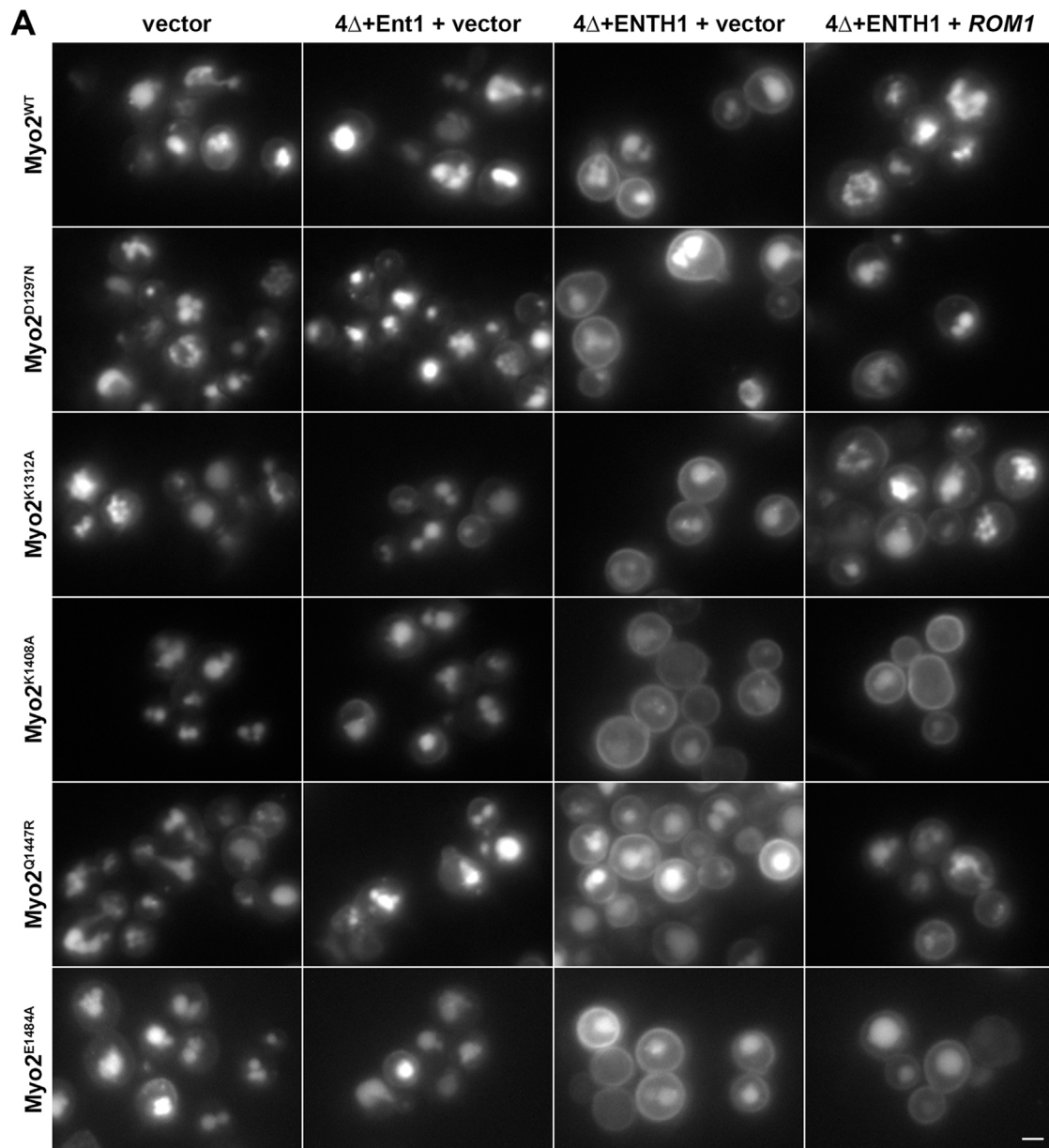
When we analyzed endocytic capacity in the same set of strains expressing Ste3-pHluorin, we observed quantitative trends that largely agreed with localization patterns of Ste3-GFP (Figure 2, B–G). In WT and 4Δ+Ent1 backgrounds with functional CME, whole-cell intensity of Ste3-pHluorin was similarly low regardless of whether the cells expressed WT Myo2 or any of the CBD mutants. Ste3-pHluorin intensity was significantly higher in all empty vector-transformed 4Δ+ENTH1 strains compared with their Myo2 CBD-matched control WT and 4Δ+Ent1 background strains, as expected for cells with defective CME. Transformation of 4Δ+ENTH1 cells expressing WT Myo2 or the D1297N, K1312A, Q1447R, or E1484A CBD mutants significantly improved Ste3-pHluorin internalization, as seen by lower fluorescence intensity compared with empty vector-transformed 4Δ+ENTH1 cells (Figure 2, B–D, F and G). In contrast, Myo2^{K1408A} 4Δ+ENTH1 cells transformed with high-copy *ROM1* were significantly brighter than empty vector-transformed cells, suggesting a possible worsening of the endocytic defect (Figure 2E). Interestingly, high-copy *ROM1* showed varying degrees of rescue in the other CBD mutants: it fully rescued Ste3-pHluorin internalization to WT or 4Δ+Ent1 levels in cells expressing Myo2 WT, D1297N, and Q1447R, but only partially improved internalization to levels that remained higher than for WT or 4Δ+Ent1 cells expressing Myo2^{K1312A} or Myo2^{E1484A}. Overall, the ability of Myo2 to transport microtubule plus ends appears to be required for CIE,

while other motor functions appear to play less prominent roles or are dispensable. Our observation that loss of mitochondrial (K1312A) or peroxisomal (E1484A) transport resulted in only partial rescue of the endocytic defect in 4Δ+ENTH1 cells by high-copy *ROM1* suggests that these functions of Myo2 are not strictly required for CIE, but may nonetheless play roles that are currently unclear. However, given that the Kar9-binding mutant (K1408A) resulted in the most prominent defect in CIE, we chose to focus on microtubule transport in this study.

Links between Myo2 and microtubule plus ends are required for CIE

Our finding that microtubule plus-end transport contributes to CIE was unexpected because the yeast microtubule cytoskeleton is thought to play limited roles in membrane traffic; however, a previous study implicated microtubules and the plus-end tracking protein Bik1 in trafficking of the v-SNARE Snc1 (Boscheron *et al.*, 2016). *tub1-Glu* and *bik1Δ* mutations caused Snc1 mislocalization reminiscent of defective endocytosis that were suppressed by Rho1 activation; thus, we further examined links between Myo2 and microtubule plus-end binding proteins. The Myo2 CBD binds Kar9, the yeast homologue of adenomatous polyposis coli (APC; Beach *et al.*, 2000). In turn, Kar9 associates with the plus-end binding protein Bim1, which is homologous to mammalian EB1. Myo2, Kar9, and Bim1 function together in a pathway required for cortical microtubule (cMT) capture which is partially redundant with a second pathway involving dynein, Bik1 (homologue of CLIP-170) and Num1 (Miller and Rose, 1998; Adames and Cooper, 2000; Lee *et al.*, 2000; Miller *et al.*, 2000; Yin *et al.*, 2000; Farkasovsky and Küntzel, 2001). Kar9 and Bim1 both additionally associate with Bik1, suggesting the possibility of cross-talk between these pathways (Moore *et al.*, 2006).

To begin examining the role of these plus-end binding proteins in CIE, we generated *kar9Δ*, *bim1Δ*, and *bik1Δ* mutants in WT, 4Δ+Ent1, and 4Δ+ENTH1 backgrounds expressing Ste3-GFP or Ste3-pHluorin. Each of the plus end transport-regulating proteins did not alter vacuolar delivery of Ste3-GFP in empty vector-transformed WT and 4Δ+Ent1 backgrounds compared with equivalent cells with no modification to plus-end binding genes (Figure 3A). As expected, Ste3-GFP was partially retained at the PM in 4Δ+ENTH1 cells as well as *kar9Δ*, *bim1Δ*, and *bik1Δ* 4Δ+ENTH1 cells with empty vector. High-copy *ROM1* appeared to improve Ste3-GFP internalization in 4Δ+ENTH1 and *bik1Δ* 4Δ+ENTH1 cells, but had little effect in *kar9Δ* or *bim1Δ* 4Δ+ENTH1 cells. When we quantified Ste3-pHluorin intensity in these backgrounds, we found that WT and 4Δ+Ent1 backgrounds were similarly dim in each case, while 4Δ+ENTH1 backgrounds were significantly brighter in comparison (Figure 3, B–E). In 4Δ+ENTH1 cells with no modification to plus-end binding genes, high-copy *ROM1* fully restored Ste3-pHluorin internalization to WT or 4Δ+Ent1 levels (Figure 3B). In contrast, high-copy *ROM1* did not reduce Ste3-pHluorin intensity in *kar9Δ* 4Δ+ENTH1 cells compared with empty vector, suggesting that the plus-end binding complex is required for CIE (Figure 3C). Ste3-pHluorin internalization was partially restored in *bim1Δ* and *bik1Δ* 4Δ+ENTH1 cells with high-copy *ROM1*, where fluorescence intensity was significantly lower than cells with empty vector, suggesting that neither gene is required for CIE (Figure 3, D and E). This was unexpected, as *ROM1* appeared to improve Ste3-GFP internalization in *bik1Δ*, but not *bim1Δ* 4Δ+ENTH1 cells (Figure 3A). Notably, the decrease in Ste3-pHluorin intensity for *bim1Δ* 4Δ+ENTH1 cells expressing high-copy *ROM1* versus empty vector (14.6% reduction) was much smaller than that of *bik1Δ* 4Δ+ENTH1 cells (47.4% reduction), suggesting a

A

| | vector | 4Δ+Ent1 + vector | 4Δ+ENTH1 + vector | 4Δ+ENTH1 + *ROM1* |

Myo2^WT

Myo2^D1297N

Myo2^K1312A

Myo2^K1408A

Myo2^Q1447R

Myo2^E1484A

B *MYO2^WT*

Ste3-pHluorin intensity (a.u.)

*** / *** / ***

vector | 4Δ+Ent1 + vector | + vector | + *ROM1* | 4Δ+ENTH1

C *MYO2^D1297N*

Ste3-pHluorin intensity (a.u.)

*** / *** / ***

vector | 4Δ+Ent1 + vector | + vector | + *ROM1* | 4Δ+ENTH1

D *MYO2^K1312A*

Ste3-pHluorin intensity (a.u.)

*** / *** / *** / #, †††

vector | 4Δ+Ent1 + vector | + vector | + *ROM1* | 4Δ+ENTH1

E *MYO2^K1408A*

Ste3-pHluorin intensity (a.u.)

* / ** / *** / ###, †††

vector | 4Δ+Ent1 + vector | + vector | + *ROM1* | 4Δ+ENTH1

F *MYO2^Q1447R*

Ste3-pHluorin intensity (a.u.)

*** / *** / ***

vector | 4Δ+Ent1 + vector | + vector | + *ROM1* | 4Δ+ENTH1

G *MYO2^E1484A*

Ste3-pHluorin intensity (a.u.)

*** / *** / *** / ###, †††

vector | 4Δ+Ent1 + vector | + vector | + *ROM1* | 4Δ+ENTH1

greater effect for *bim1Δ* than for *bik1Δ*. Combined with the PM retention of Ste3-GFP in *bim1Δ* 4Δ+ENTH1 cells, it is thus possible that Bik1 plays a weaker role in CIE, or that the two proteins share overlapping function through their roles in distinct cMT capture pathways or interactions with Kar9. Unfortunately, *bim1Δ bik1Δ* cells are inviable, so we were unable to directly test this possibility (Schwartz *et al.*, 1997). Nonetheless, these data suggest that Kar9 and microtubule plus-end binding proteins contribute to CIE.

Stability of cytoplasmic microtubules contributes to CIE

Given our observations that Myo2- and Kar9-dependent transport of microtubules is required for CIE in yeast, we decided to more directly test the involvement of microtubules in this process. We previously showed that actin is required for CIE in addition to its established role in CME by treating cells with the actin-depolymerizing drug Latrunculin A (LatA; Prosser *et al.*, 2011). Using WT, 4Δ+Ent1, and 4Δ+ENTH1 cells transformed with empty vector, as well as 4Δ+ENTH1 cells with high-copy *ROM1*, we examined Ste3-GFP localization in vehicle (DMSO), LatA, and nocodazole-treated cells to determine whether microtubule depolymerization would also affect Rom1-dependent internalization (Figure 4A). As seen previously, 2 h treatment with LatA inhibited endocytosis in all strains, where Ste3-GFP was almost completely retained at the PM (Figure 4A; Prosser *et al.*, 2011). In contrast, DMSO-treated controls showed the expected pattern of primarily vacuolar Ste3-GFP in WT and 4Δ+Ent1 cells with empty vector, prominent PM retention in 4Δ+ENTH1 cells with empty vector, and improved internalization in 4Δ+ENTH1 with high-copy *ROM1*. Ste3-GFP showed similar localization in nocodazole- and DMSO-treatment conditions for WT, 4Δ+Ent1, and 4Δ+ENTH1 cells with empty vector. However, 4Δ+ENTH1 cells with high-copy *ROM1* appeared to show weaker Ste3-GFP internalization with nocodazole treatment compared with DMSO. As evidence that our LatA and nocodazole treatments were effective, we also examined localization of the cortical actin patch protein Abp1 and the alpha-tubulin protein Tub1. As shown in Figure 4B, Abp1-GFP localized prominently to cortical actin patches in DMSO- and nocodazole-treated cells, but completely redistributed to the cytoplasm with LatA treatment. GFP-Tub1 localized to spindle pole bodies, cytoplasmic microtubule structures, and the mitotic spindle in DMSO- and LatA-treated cells, but cytoplasmic and spindle microtubules were not observed with nocodazole treatment. GFP-Tub1 remained observable at spindle pole bodies that were primarily located on the mother side of nocodazole-treated budding cells, consistent with previous findings (Cuschieri *et al.*, 2006; Lee *et al.*, 2013). In further support of our findings, we also performed quantitative experiments using Ste3-pHluorin to assess whether high-copy *ROM1* could improve cargo internalization in LatA- and nocodazole-treated cells. As shown in Figure 4C, whole-cell Ste3-pHluorin levels were significantly higher in 4Δ+ENTH1 cells with empty vector compared with WT or 4Δ+Ent1 cells with empty

vector in DMSO, LatA, and nocodazole treatment conditions, consistent with impaired endocytosis when CME is blocked. In DMSO-treated 4Δ+ENTH1 cells with high-copy *ROM1*, Ste3-pHluorin intensity was significantly lower than 4Δ+ENTH1 cells with empty vector, as expected. However, high-copy *ROM1* failed to improve Ste3-pHluorin intensity levels in cells treated with either LatA or with nocodazole, suggesting that both actin and microtubules participate in CIE.

Because force must be exerted at the PM for endocytosis to occur, we further reasoned that stability of cytoplasmic microtubules is required for their role in CIE. The kinesin-related motors Kip2 and Kip3 play opposing roles in regulating cytoplasmic microtubule stabilization, where Kip2 inhibits catastrophe and promotes microtubule polymerization, while Kip3 destabilizes microtubules (Miller *et al.*, 1998). Thus, *kip2Δ* results in destabilization of cytoplasmic microtubules, while *kip3Δ* causes their hyper-stabilization. We reasoned that loss of cytoplasmic microtubules in *kip2Δ* cells would impair the CIE pathway if they contribute to internalization at the PM; in contrast, stabilization of cytoplasmic microtubules in *kip3Δ* cells might facilitate CIE even in 4Δ+ENTH1 cells with an empty vector, possibly by enhancing the number or stability of cMT sites at the PM. Thus, we generated *kip2Δ* and *kip3Δ* strains in WT, 4Δ+Ent1 and 4Δ+ENTH1 backgrounds, and used these to examine Ste3-GFP localization. Neither *kip2Δ* nor *kip3Δ* altered the predominantly vacuolar localization of Ste3-GFP in WT or 4Δ+Ent1 backgrounds with empty vector, as expected for strains with functional CME (Figure 5A). In *kip2Δ* 4Δ+ENTH1 cells with empty vector, Ste3-GFP largely accumulated at the PM, consistent with a block in CME. Transformation of *kip2Δ* 4Δ+ENTH1 cells with high-copy *ROM1* did not noticeably improve Ste3-GFP internalization. Interestingly, empty vector-transformed *kip3Δ* 4Δ+ENTH1 cells showed lower PM accumulation of Ste3-GFP with correspondingly higher vacuolar delivery, and high-copy *ROM1* gave similar distribution of the cargo. These findings correlate with microtubule stability: we were unable to observe cytoplasmic microtubules in *kip2Δ* cells expressing GFP-Tub1 compared with WT cells; in contrast, *kip3Δ* cells showed exaggerated cytoplasmic microtubules that appeared to wrap around the cell cortex (Figure 5B).

Quantification of Ste3-pHluorin intensity in *kip2Δ* and *kip3Δ* strains supported our observations of Ste3-GFP localization. For *kip2Δ* or *kip2Δ* 4Δ+Ent1 cells with empty vector, whole-cell Ste3-pHluorin intensity was similarly low, while *kip2Δ* 4Δ+ENTH1 cells with empty vector were significantly brighter (Figure 5C, compared with control cells in Figure 3B). Consistent with a requirement for Kip2 in CIE, transformation of *kip2Δ* 4Δ+ENTH1 cells with high-copy *ROM1* failed to improve internalization, as shown by similar brightness to *kip2Δ* 4Δ+ENTH1 cells with empty vector. Deletion of *KIP3* in 4Δ+ENTH1 cells with empty vector also resulted in a small, but significant increase in Ste3-pHluorin intensity compared with *kip3Δ*

FIGURE 2: Effect of Myo2 CBD mutation on clathrin-independent endocytosis. WT Myo2 or CBD mutants (D1297N, K1312A, K1408A, Q1447R, and E1484A) expressed as the sole source of Myo2 in WT (vector), 4Δ+Ent1 and 4Δ+ENTH1 backgrounds were transformed with vector or high-copy *ROM1* as indicated. (A) Cells expressing Ste3-GFP from the endogenous locus were imaged by fluorescence microscopy. (B–G) Quantification of whole-cell fluorescence intensity in cells expressing Ste3-pHluorin transformed as in *A*. (B) Myo2^{WT} ($n = 46$, $n = 52$, $n = 40$ and $n = 40$, respectively). (C) Myo2^{D1297N} ($n = 43$, $n = 41$, $n = 49$ and $n = 41$, respectively). (D) Myo2^{K1312A} ($n = 53$, $n = 47$, $n = 48$ and $n = 63$, respectively). (E) Myo2^{K1408A} ($n = 46$, $n = 55$, $n = 52$ and $n = 48$, respectively). (F) Myo2^{Q1447R} ($n = 59$, $n = 52$, $n = 58$ and $n = 65$, respectively). (G) Myo2^{E1484A} ($n = 51$, $n = 41$, $n = 41$ and $n = 54$, respectively). Mean ± SD; *$p < 0.05$, **$p < 0.01$, ***$p < 0.001$; #$p < 0.05$ and ###$p < 0.001$ compared with WT; †††$p < 0.001$ compared with 4Δ+Ent1. Scale bar: 2 µm.
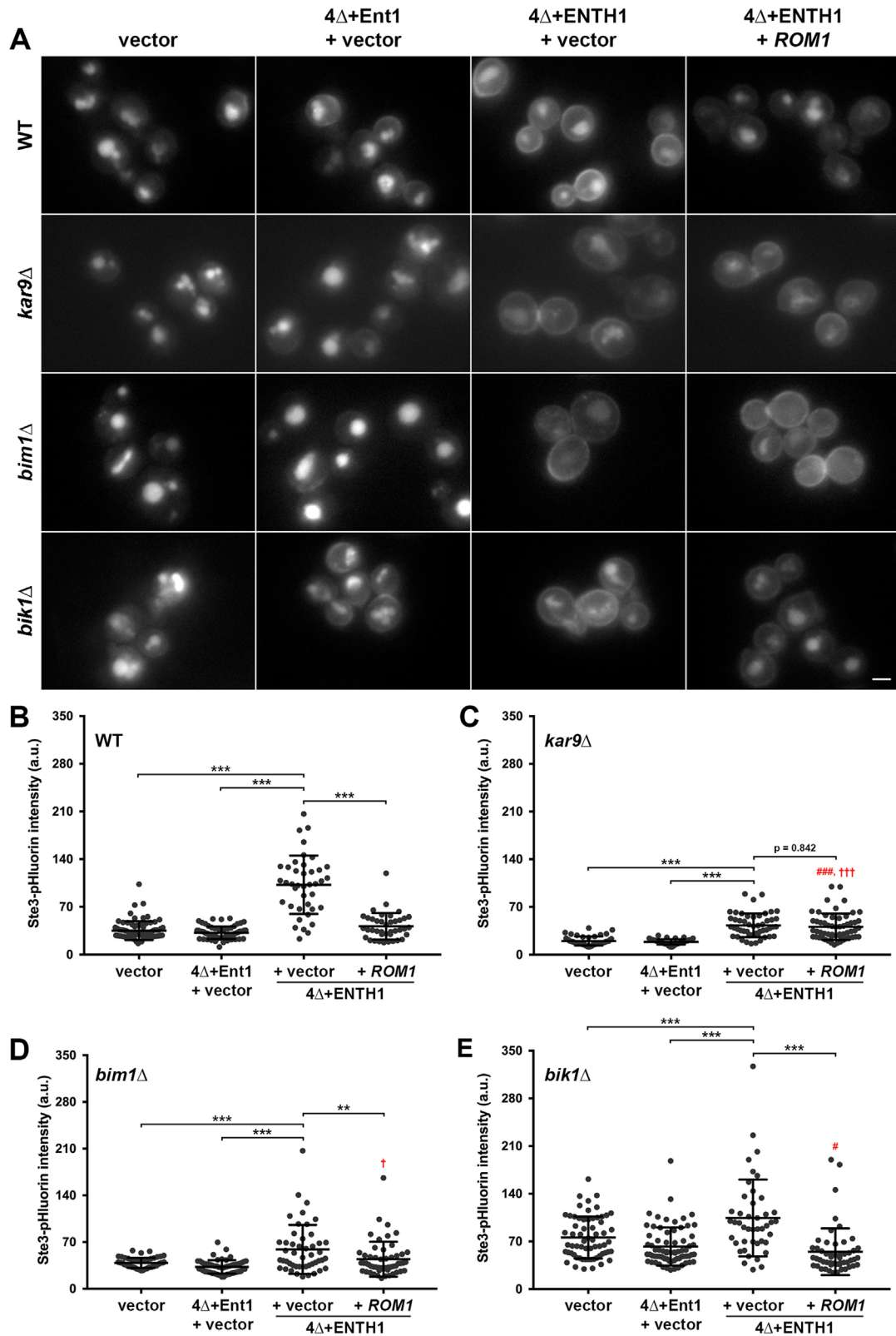
FIGURE 3: Requirement for microtubule plus end-binding proteins in clathrin-independent endocytosis. WT (vector), 4Δ+Ent1 and 4Δ+ENTH1 backgrounds were transformed with vector or high-copy *ROM1* as indicated. *kar9Δ*, *bim1Δ*, and *bik1Δ* were generated in the same strains. (A) Cells expressing Ste3-GFP from the endogenous locus were imaged by fluorescence microscopy. (B–E) Quantification of whole-cell fluorescence intensity in cells expressing Ste3-pHluorin transformed as in *A*. (B) WT, 4Δ+Ent1 and 4Δ+ENTH1 backgrounds with no additional modifications ($n = 77$, $n = 65$, $n = 40$ and $n = 40$, respectively). (C) *kar9Δ* ($n = 45$, $n = 51$, $n = 50$ and $n = 57$, respectively). (D) *bim1Δ* ($n = 84$, $n = 84$, $n = 50$ and $n = 63$, respectively). (E) *bik1Δ* ($n = 64$, $n = 70$, $n = 44$ and $n = 52$, respectively). Mean ± SD; ***$p < 0.001$; #$p < 0.05$ and ###$p < 0.001$ compared with WT; †$p < 0.05$ and †††$p < 0.001$ compared with 4Δ+Ent1. Scale bar: 2 μm.
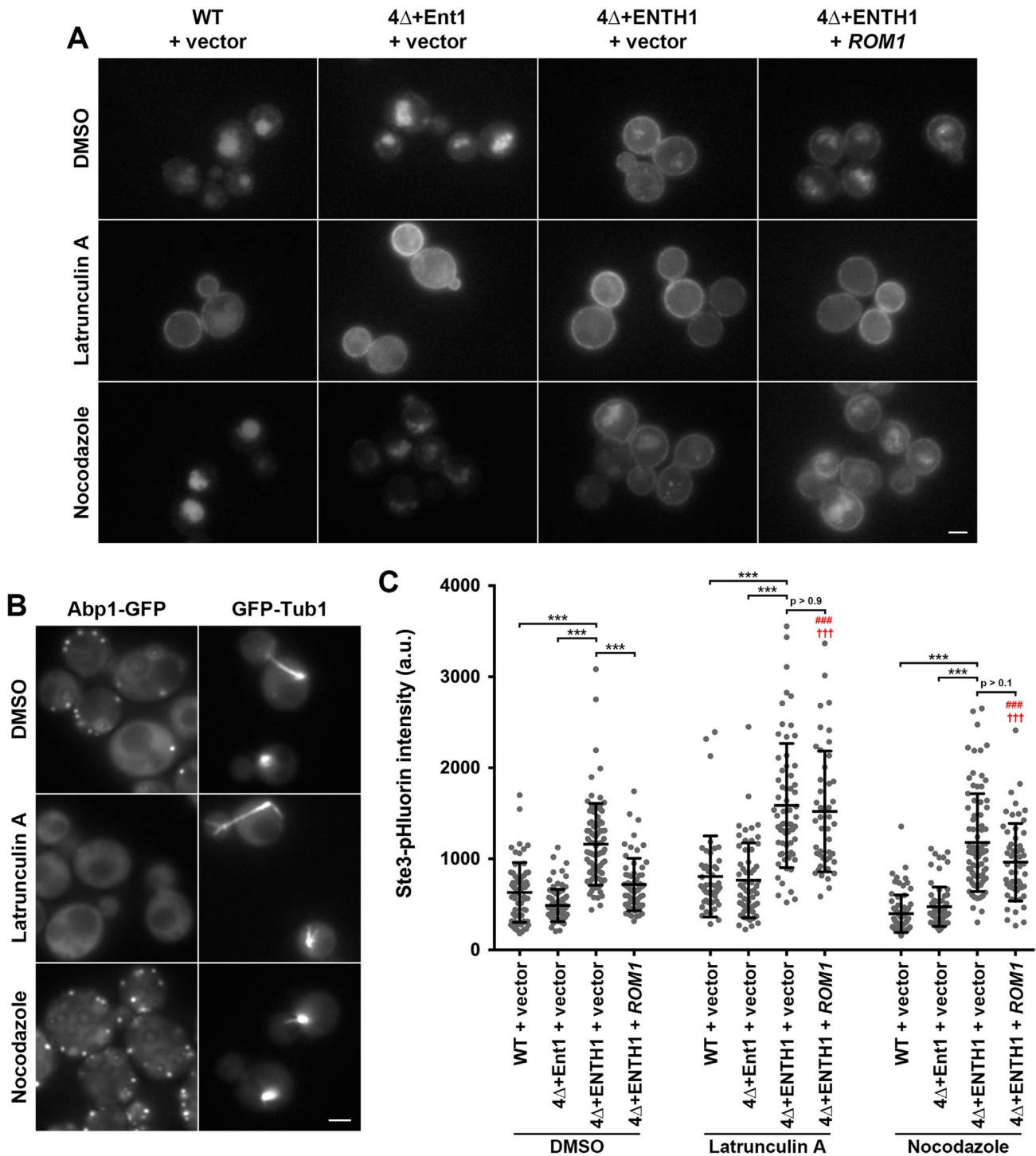
FIGURE 4: Requirement for actin and microtubules in clathrin-independent endocytosis. (A) WT, 4Δ+Ent1 and 4Δ+ENTH1 cells expressing Ste3-GFP from the endogenous locus were transformed with vector or high-copy *ROM1* as indicated. Cells grown to midlogarithmic phase were treated with vehicle (DMSO), 200 µM LatA, or 15 µg/ml Nocodazole for 2 h before imaging by fluorescence microscopy. (B) WT cells expressing Abp1-GFP or GFP-Tub1 were subjected to the same treatment as in panel *A*, and imaged by fluorescence microscopy to demonstrate the effectiveness of LatA and Nocodazole treatments. Scale bars: 2 µm. (C) Quantification of whole-cell fluorescence intensity in cells expressing Ste3-pHluorin instead of Ste3-GFP and treated with DMSO, LatA or Nocodazole as in panel *A* (n > 46 for all conditions). Mean ± SD; ***p < 0.001; ###*p* < 0.001 compared with WT; †††*p* < 0.001 compared with 4Δ+Ent1.

or *kip3Δ* 4Δ+Ent1 cells (Figure 5D); however, this increase (33.7% for *kip3Δ* 4Δ+ENTH1 compared with *kip3Δ* with empty vector) was much smaller than seen when comparing *kip2Δ* to *kip2Δ* 4Δ+ENTH1

with empty vector (99.2% increase). Transformation of *kip3Δ* 4Δ+ENTH1 cells with high-copy *ROM1* resulted in Ste3-pHluorin intensity levels that were indistinguishable from *kip3Δ*, *kip3Δ* 4Δ+Ent1,
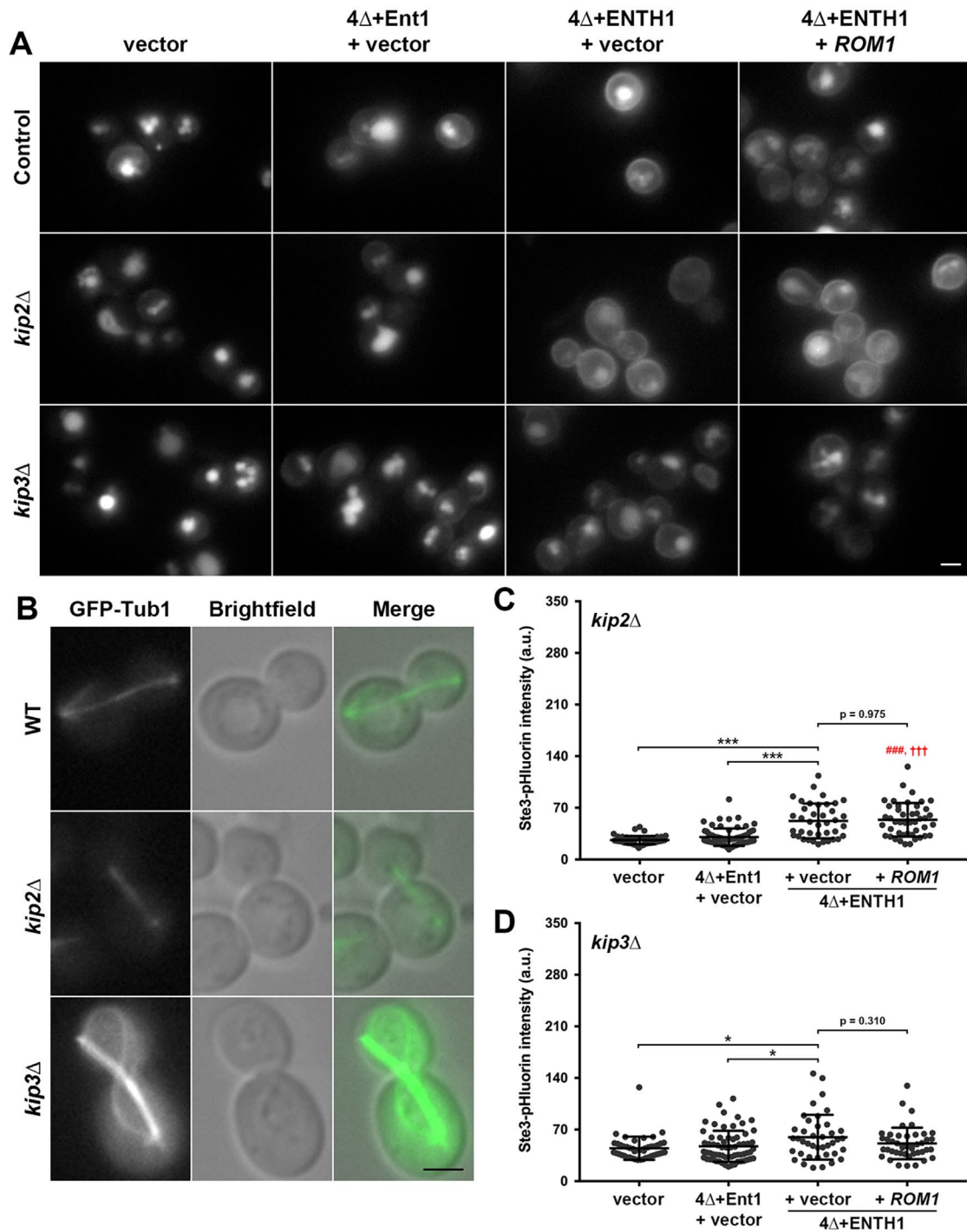
FIGURE 5: Role of cytoplasmic-microtubule stability in clathrin-independent endocytosis. Cytoplasmic microtubule-destabilizing (*kip2Δ*) and -stabilizing (*kip3Δ*) mutants generated in WT (vector), 4Δ+Ent1 and 4Δ+ENTH1 backgrounds were transformed with vector or high-copy *ROM1* as indicated. (A) Control, *kip2Δ* and *kip3Δ* cells expressing Ste3-GFP from the endogenous locus were imaged by fluorescence microscopy. (B) Fluorescence microscopy of GFP-Tub1 expressed in large-budded WT, *kip2Δ*, and *kip3Δ* cells, with brightfield and merged panels to demonstrate microtubule localization. (C and D) Quantification of whole-cell fluorescence intensity in cells expressing Ste3-pHluorin transformed as in A. (C) *kip2Δ* ($n = 49$, $n = 69$, $n = 39$ and $n = 45$, respectively). (D) *kip3Δ* ($n = 46$, $n = 65$, $n = 40$ and $n = 44$, respectively). Mean ± SD; ***$p < 0.001$; ###$p < 0.001$ compared with WT; †††$p < 0.001$ compared with 4Δ+Ent1. The corresponding control quantification for Ste3-pHluorin internalization is shown in Figure 3B. Scale bars: 2 μm.

or *kip3Δ* 4Δ+ENTH1 cells with empty vector. Taken together, these experiments demonstrate that stability of cytoplasmic microtubules is required for CIE, and that their stabilization may increase clathrin-independent endocytosis in yeast.

Dynein and dynactin are required for CIE in yeast

Our findings that cytoplasmic microtubules, and Myo2-dependent transport of microtubule plus ends, contribute to CIE prompted us next to examine whether the minus-end directed microtubule motor

dynein and its cofactor dynactin are also needed. As microtubule plus ends are transported along actin cables, dynein and dynactin are targeted to the plus end through an interaction between the dynein heavy chain (Dyn1) and Pac1 (homologue of the mammalian lissencephaly protein, LIS1), which in turn binds to Bik1 (Sheeman et al., 2003). To explore the role of this protein module in CIE, we focused on four deletions: dyn1Δ (dynein heavy chain) and pac11Δ (dynein intermediate chain) which cause a loss of dynein function, nip100Δ (dynactin p150^Glued subunit) which causes a loss of dynactin function, and pac1Δ which disrupts plus-end tracking of dynein/dynactin (Geiser et al., 1997; Sheeman et al., 2003). We generated each of these deletions in WT, 4Δ+Ent1, and 4Δ+ENTH1 backgrounds, and subsequently examined Ste3-GFP localization and the effect of high-copy ROM1 on Ste3 internalization in the CME-defective 4Δ+ENTH1 strain. As expected for each of these deletions in WT and 4Δ+Ent1 backgrounds transformed with empty vector, Ste3-GFP was efficiently delivered to the vacuole, indicating that loss of dynein/dynactin function or plus-end tracking are not required for cargo internalization when CME is functional (Figure 6A). In dyn1Δ, pac11Δ, nip100Δ, and pac1Δ 4Δ+ENTH1 cells transformed with empty vector, Ste3-GFP localized prominently at the PM, indicating a reduction in internalization. When each of the corresponding 4Δ+ENTH1 backgrounds were instead transformed with high-copy ROM1, Ste3-GFP retention at the PM was similar to cells with empty vector. Quantification of Ste3-pHluorin intensity confirmed the endocytic effects observed with Ste3-GFP: dyn1Δ, pac11Δ, nip100Δ, and pac1Δ in WT and 4Δ+Ent1 backgrounds with empty vector had similarly low fluorescence intensity, which was significantly higher in the 4Δ+ENTH1 background (Figure 6, B–E, compared with control cells in Figure 3B). Transformation of dyn1Δ, pac11Δ, nip100Δ, and pac1Δ 4Δ+ENTH1 cells with high-copy ROM1 failed to reduce the elevated Ste3-pHluorin intensity, indicating that Rom1 was no longer able to improve cargo internalization in the absence of dynein/dynactin or Pac1 function.

cMT capture is required for CIE in yeast

Once Myo2 delivers microtubule plus ends to the cell cortex, an offloading event occurs in which the dynein intermediate chain Pac11 (in complex with microtubules) associates with Num1, a protein that forms stable patches at the cell cortex (Lee et al., 2003, 2005). These patches are sites of cMT anchoring, where Num1 binding to Pac11 leads to dynein activation by relieving the inhibitory activity of Pac1. Activated dynein is a minus-end directed motor, which pulls on the cytoplasmic microtubule to position the nucleus at the neck of large-budded cells in preparation for mitosis (Kahana et al., 1998). Because our data indicate that cytoplasmic microtubules and dynein/dynactin are involved in CIE, we generated num1Δ strains to test whether cMT anchoring is also required. As shown in in Figure 7A, num1Δ did not affect vacuolar Ste3-GFP delivery in WT and 4Δ+Ent1 backgrounds transformed with empty vector, indicating that Num1 is not required for cargo internalization when CME is functional. In contrast, Ste3-GFP was prominently retained at the PM in num1Δ 4Δ+ENTH1 cells with empty vector, and this defective localization was not corrected by transformation with high-copy ROM1. Similarly, quantification of Ste3-pHluorin intensity in num1Δ cells showed low fluorescence in WT and 4Δ+Ent1 backgrounds with empty vector, in agreement with vacuolar localization seen for Ste3-GFP (Figure 7B, compared with control cells in Figure 3B). As expected, Ste3-pHluorin intensity was significantly higher in num1Δ 4Δ+ENTH1 cells with empty vector. Transformation of num1Δ 4Δ+ENTH1 cells with high-copy ROM1 failed to improve the elevated-fluorescence intensity of Ste3-pHluorin compared with empty
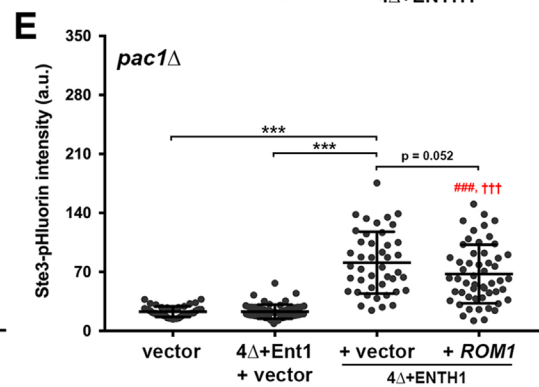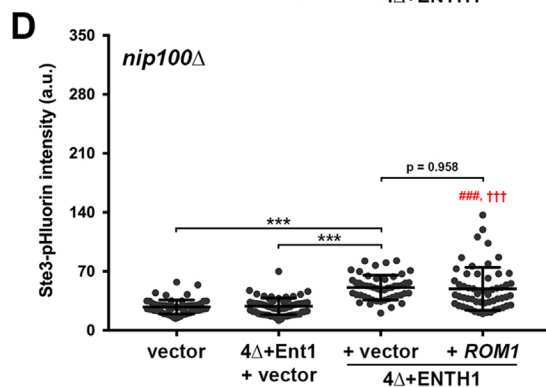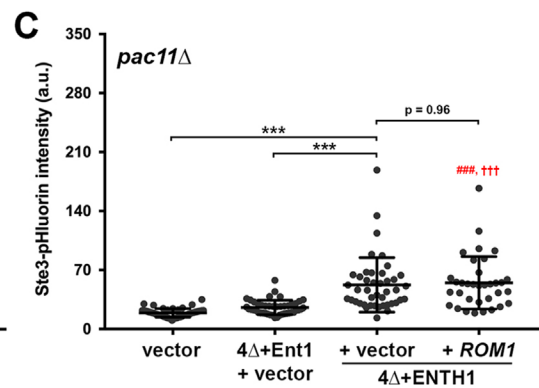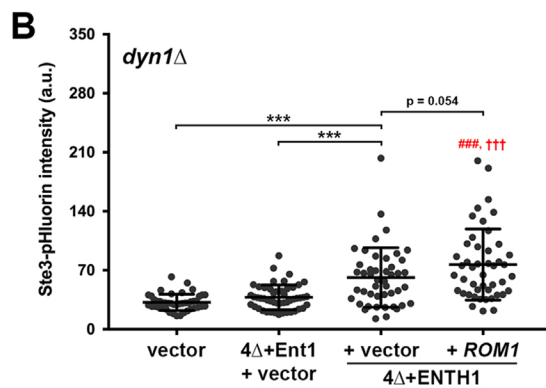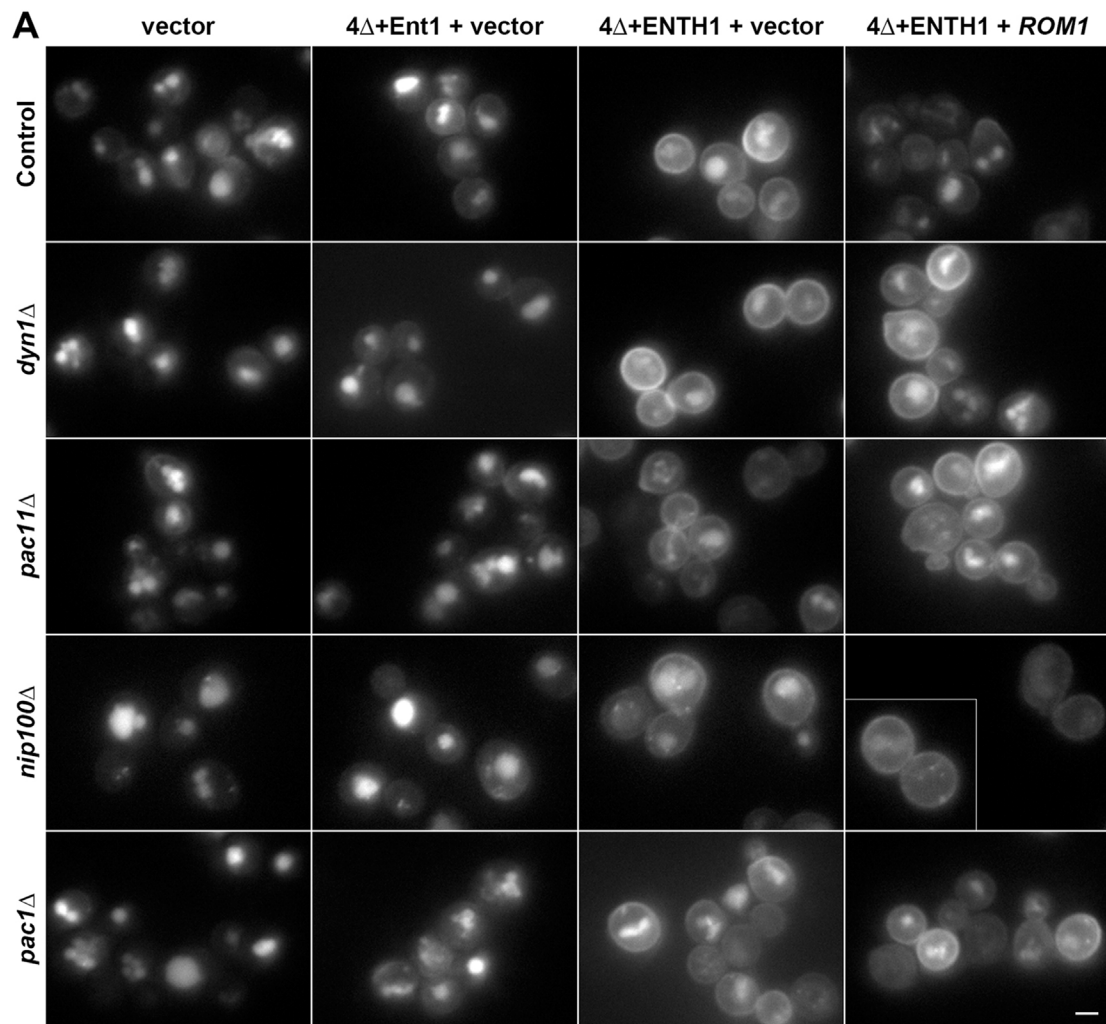
vector; in fact, ROM1-transformed cells were significantly brighter than the vector control in num1Δ 4Δ+ENTH1 cells, similar to myo2^K1408A 4Δ+ENTH1 cells defective in Myo2-dependent microtubule transport (Figure 2E). Thus, cMT capture and anchoring, in addition to transport of cytoplasmic microtubules, appears to be required for CIE.

In our examination of the role of microtubules and cMT capture machinery in CIE, we considered the possibility that mitotic spindle positioning may be altered in cells with defective CME or that strains with defective CIE may share a spindle orientation defect. Thus, we generated strains with a chromosomal integration of GFP-TUB1, expressed from the TUB1 promoter, at the LYS2 gene locus. WT, 4Δ+Ent1 and 4Δ+ENTH1 cells with empty vector or high-copy ROM1 all had similar microtubule morphologies in unbudded and budded cells, with no obvious spindle misorientation, suggesting that inhibition of CME or overexpression of ROM1 did not alter the microtubule cytoskeleton (Supplemental Figure S3A). Additionally, we examined GFP-Tub1 in a variety of other strains harboring deletions in cMT transport and capture. With these strains, we observed spindle orientation similar to WT cells in some cases (kar9Δ, bim1Δ, bik1Δ, and pac1Δ), but a severe spindle misalignment in cells with defective dynein, dynactin, or cMT anchoring (dyn1Δ, pac11Δ, nip100Δ, and num1Δ; Supplemental Figure S3B). All spindle orientation phenotypes were similar when these mutations were generated in the 4Δ+Ent1 and 4Δ+ENTH1 backgrounds (unpublished data). Our observations agree with numerous prior studies showing spindle misalignment in many mutants with defective cMT capture and nuclear positioning (Eshel et al., 1993; Farkasovsky and Küntzel, 1995; Kahana et al., 1998; Miller and Rose, 1998; Stuchell-Brereton et al., 2011). Notably, spindle misalignment is not necessarily required for a role of these proteins in CIE, because kar9Δ and pac1Δ, which had normal spindle orientation, both prevented Rom1-dependent activation of CIE in 4Δ+ENTH1 cells (Lee et al., 2003; Anderson et al., 2022). Moreover, we previously showed that Bni1 is required downstream of Rho1 for CIE, and we did not observe spindle orientation defects in bni1Δ cells (Supplemental Figure S3C).

DISCUSSION

Although a variety of CIE pathways have now been observed in most eukaryotes, the molecular mechanisms governing CIE have remained elusive compared with our understanding of CME. Many aspects of CIE have not yet been addressed in detail, due in part to the relatively small number of proteins implicated in CIE and a lack of tools to study these pathways. In turn, this leaves open questions about: 1) the degree of overlap in protein machinery between different CIE pathways, or between CME and CIE; 2) the relative level of complexity required to generate clathrin-coated and clathrin-independent vesicles; 3) mechanisms for generating the force required for membrane deformation, curvature stabilization and vesicle scission in the absence of a clathrin coat; 4) how cells select and sort cargo into different endocytic pathways; and 5) the relative contribution of CME and CIE to cargo and membrane internalization under a variety of physiological conditions and stimuli.

Our previous discovery of the first CIE pathway observed in budding yeast has provided us with a genetically tractable system to begin answering these questions (Prosser et al., 2011). This earlier study identified a signaling cascade involving the cell wall stress sensor Mid2, the Rho1 GEFs Rom1 and Rom2, the Rho1 GTPase and its effector Bni1 (along with Bni1-recruiting and -activating proteins in the polarisome) as central components of CIE in yeast. Moreover, the early-acting CME machinery protein Syp1 contributes to both clathrin-dependent and clathrin-independent internalization
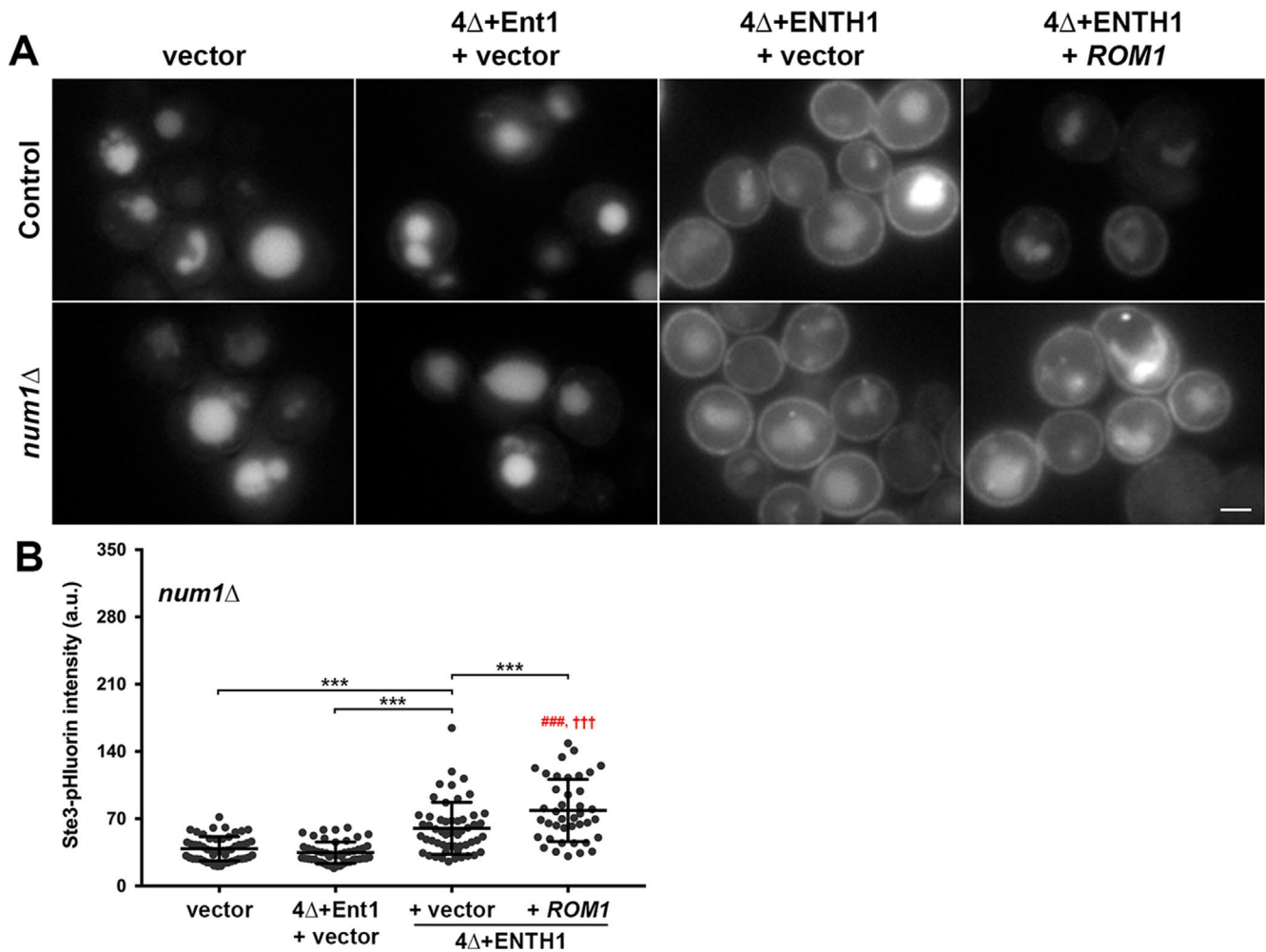
A

| | vector | 4Δ+Ent1 + vector | 4Δ+ENTH1 + vector | 4Δ+ENTH1 + *ROM1* |

Control

dyn1Δ

pac11Δ

nip100Δ

pac1Δ

B *dyn1Δ*

Ste3-pHluorin intensity (a.u.)

*** *** p = 0.054

###, †††

vector | 4Δ+Ent1 + vector | + vector | + *ROM1*
4Δ+ENTH1

C *pac11Δ*

Ste3-pHluorin intensity (a.u.)

*** *** p = 0.96

###, †††

vector | 4Δ+Ent1 + vector | + vector | + *ROM1*
4Δ+ENTH1

D *nip100Δ*

Ste3-pHluorin intensity (a.u.)

*** *** p = 0.958

###, †††

vector | 4Δ+Ent1 + vector | + vector | + *ROM1*
4Δ+ENTH1

E *pac1Δ*

Ste3-pHluorin intensity (a.u.)

*** *** p = 0.052

###, †††

vector | 4Δ+Ent1 + vector | + vector | + *ROM1*
4Δ+ENTH1

FIGURE 7: Requirement for the cMT capture protein Num1 in clathrin-independent endocytosis. *num1Δ* in WT (vector), 4Δ+Ent1 and 4Δ+ENTH1 backgrounds were transformed with vector or high-copy *ROM1* as indicated. (A) Control and *num1Δ* cells expressing Ste3-GFP from the endogenous locus were imaged by fluorescence microscopy. (B) Quantification of whole-cell fluorescence intensity in cells expressing Ste3-pHluorin transformed as in *A* ($n = 52$, $n = 49$, $n = 54$ and $n = 40$, respectively). Mean ± SD; ***$p < 0.001$; ###$p < 0.001$ compared with WT; †††$p < 0.001$ compared with 4Δ+Ent1. The corresponding control quantification for Ste3-pHluorin internalization is shown in Figure 3B. Scale bar: 2 μm.

of cargos such as the di- and tripeptide transporter Ptr2 (Apel *et al.*, 2017). Syp1 contains an N-terminal Fes/CIP4 homology-Bin/Amphiphysin/Rvs (F-BAR) domain involved in sensing and inducing membrane curvature and a cargo-binding μ-homology domain (μHD) at its C-terminus, both of which are required for localization to and function at CME sites (Reider *et al.*, 2009). Syp1 directly binds to and promotes internalization of Mid2, likely through CME because we have not observed Mid2 internalization under conditions where CIE

promotes uptake of Ste3 or other cargos (D. Prosser, unpublished data); thus, it is unclear whether Syp1 plays mechanistically similar roles in CME and CIE. Finally, α-arrestins, which act as cargo-selective adaptors for the ubiquitin ligase Rsp5 during CME, also participate in CIE through interactions with proteins such as Rom2 and Rho1 (Prosser *et al.*, 2015). Rsp5 and its interaction with α-arrestins is not required for CIE, even though the α-arrestins retain their cargo-selective roles in directing proteins to CIE. While the majority

FIGURE 6: Requirement for dynein, dynactin, and microtubule plus-end tracking proteins in clathrin-independent endocytosis. Dynein (*dyn1Δ* and *pac11Δ*), dynactin (*nip100Δ*) and plus-end tracking (*pac1Δ*) mutants generated in WT (vector), 4Δ+Ent1 and 4Δ+ENTH1 backgrounds were transformed with vector or high-copy *ROM1* as indicated. (A) Control, *dyn1Δ*, *pac11Δ*, *nip11Δ*, and *pac1Δ* cells expressing Ste3-GFP from the endogenous locus were imaged by fluorescence microscopy. (B–E) Quantification of whole-cell fluorescence intensity in cells expressing Ste3-pHluorin transformed as in A. (B) *dyn1Δ* ($n = 44$, $n = 50$, $n = 46$ and $n = 46$, respectively). (C) *pac11Δ* ($n = 47$, $n = 45$, $n = 43$ and $n = 34$, respectively). (D) *nip100Δ* ($n = 61$, $n = 67$, $n = 49$ and $n = 58$, respectively). (E) *pac1Δ* ($n = 42$, $n = 59$, $n = 43$ and $n = 53$, respectively). Mean ± SD; ***$p < 0.001$; ###$p < 0.001$ compared with WT; †††$p < 0.001$ compared with 4Δ+Ent1. The corresponding control quantification for Ste3-pHluorin internalization is shown in Figure 3B. Scale bar: 2 μm.
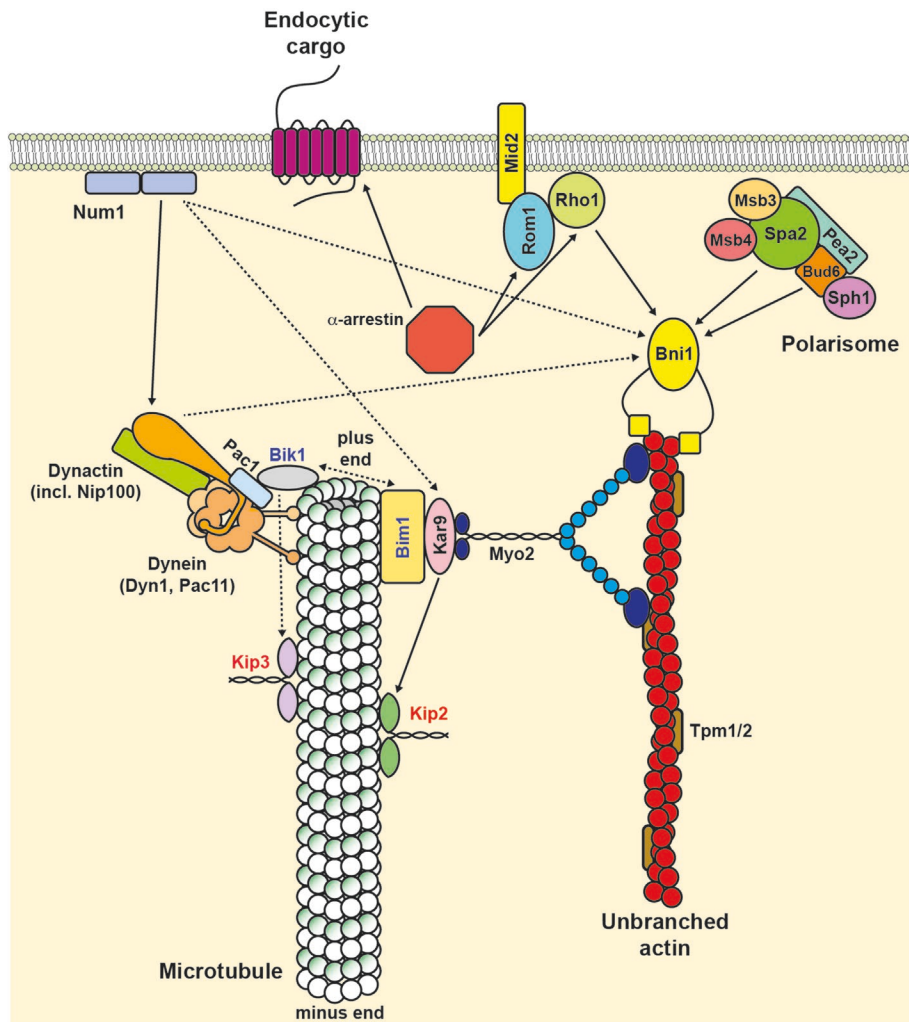
FIGURE 8: Model of protein modules involved in yeast clathrin-independent endocytosis. We previously identified several signaling modules and/or protein transport complexes that play roles in clathrin-independent endocytosis, including a cell wall stress-sensing module (Mid2, Rom1, Rho1), the polarisome (including Bni1, Bud6, and Spa2), unbranched actin filaments stabilized by tropomyosins (Tpm1 and Tpm2; Prosser et al., 2011). Here, we add Myo2, proteins involved in microtubule plus-end transport (Kar9, and possibly Bim1 and/or Bik1 which are noted in blue text to indicate potential overlapping functions), cytoplasmic microtubules and kinesin-related proteins involved in their stability (Kip2 and Kip3, noted in red text as they may exert indirect effects by regulating cytoplasmic microtubule stability), dynein (including Dyn1 and Pac11), dynactin (including Nip100), microtubule plus-end tracking proteins (Pac1), and proteins involved in cMT capture (Num1) as additional factors that contribute to CIE. To date, none of these additional proteins have defined roles in CME.

ing of the v-SNARE Snc1, where mutations in Tub1 or Bik1 caused PM accumulation of Snc1 reminiscent of the endocytosis-defective Snc1[end-] mutant (Lewis et al., 2000; Boscheron et al., 2016). Importantly, Snc1 mislocalization in tub1-Glu and bik1Δ mutants were corrected by expression of constitutively active Rho1[G19V]. This suggests a possible role for CIE in the observed effects, although contributions of CME cannot be ruled out. In our study, Bik1 was not required for CIE of Ste3-GFP (Figure 3), which might be explained by overlapping functions with Bim1 or other components of microtubule plus-end binding or tracking. Alternatively, specific endocytic cargos may physically associate with different proteins involved in CIE and/or microtubule regulation to allow recruitment into an endocytic carrier, either directly or indirectly through proteins such as α-arrestins. For example, the α-arrestin Bul2 associates with the dynactin subunit Nip100, which may allow direct links between cargos and microtubule-based transport machinery (Wang et al., 2012). As we do not yet understand how cargo is selected into CIE pathways, identifying proteins that serve as CIE cargo-selective adaptors will be an interesting future direction.

Separate from the role of Bik1 and tubulin in Snc1 trafficking, another study identified a role for the dynein light chain-family protein Tda2 in CME (Farrell et al., 2017). Rather than acting with microtubules and dynein, this novel role for Tda2 appears to rely on formation of a complex with Aim21 and the actin-capping proteins Cap1 and Cap2, leading to association with the CME protein Bbc1 and subsequent regulation of Arp2/3-dependent actin polymerization at cortical actin patches. Although these findings do not rule out a relationship between Tda2 and microtubules distinct from its contribution to CME, it is unlikely that Tda2 participates in CIE, because high-copy *ROM1* promotes Ste3-GFP internalization in *aim21Δ* 4Δ+ENTH1 cells (D. Prosser, unpublished data).

of yeast CME proteins tested to date are not required for CIE, these prior findings demonstrate that limited sets of proteins participate in both pathways.

The current study expands our understanding of CIE in yeast by identifying additional components of the pathway: the type V myosin Myo2, microtubules and plus-end binding proteins (Kar9, and possibly Bim1 and Bik1), regulators of cytoplasmic microtubule stability (Kip2 and Kip3), cMT capture (Num1), and dynein/dynactin (Dyn1, Pac11, and Nip100; Figure 8). None of these proteins have been previously implicated in CME to our knowledge, and membrane trafficking roles for microtubules or microtubule-based motors remain largely undefined in yeast. Notably, tubulin and the plus-end tracking protein Bik1 were reported to play roles in traffick-

While our findings implicate Myo2 as the primary myosin involved in CIE, we also observed a prominent endocytic defect in *myo3Δ myo5Δ* cells that was only weakly improved by high-copy expression of *ROM1* (Supplemental Figure S1, C and D). At the present time, we cannot rule out a direct role for Myo3 and Myo5 in CIE; however, both of the yeast type I myosins appear to localize exclusively to cortical actin patches, which show aberrant behavior that is not corrected under conditions that promote CIE (Sun et al., 2006; Barker et al., 2007; Prosser et al., 2011, 2015). Because our characterization of yeast CIE to date suggests that cortical actin patches are not involved in clathrin-independent internalization, we instead speculate that the weak effect of high-copy *ROM1* in *myo3Δ myo5Δ* cells may be due to loss of actin cables (Supplemental Figure S1E;

Goodson *et al.*, 1996; Anderson *et al.*, 1998), as unbranched actin filaments generated by the formin Bni1 are bundled into cables that are required for CIE (Prosser *et al.*, 2011). Consistent with this idea, both actin cables and actin patches appear to compete for G-actin monomers from the same cytoplasmic pool (Burke *et al.*, 2014; Suarez *et al.*, 2015). Thus, accumulation of F-actin in aberrant patches in *myo3Δ myo5Δ* cells, as assessed by phalloidin staining, may be indicative of a depletion of actin monomers available for formation of actin cables necessary for organelle and vesicle transport, as well as for CIE. Our future studies will examine the relationship between type I myosins and both CME and CIE in greater detail.

The degree of similarity between yeast and mammalian CIE remains a major unresolved question, in large part because of the limited set of proteins linked to any CIE pathway. As we add to the number of proteins involved in yeast CIE, it is tempting to speculate on how these relate to pathways in higher eukaryotes. Studies of several different pathways have identified roles for homologues of proteins involved in yeast CIE. For example, clathrin-independent ultrafast endocytosis occurs at synapses in mammals and *C. elegans*, and requires actin polymerization and formins (Bni1 in yeast; Watanabe *et al.*, 2013a, b; Soykan *et al.*, 2017). Additionally, FEME utilizes microtubules and dynein for inward transport of tubular endocytic carriers, as does clathrin-independent internalization of cholera toxin (Boucrot *et al.*, 2015; Day *et al.*, 2015; Watanabe and Boucrot, 2017; Casamento and Boucrot, 2020; Ferreira *et al.*, 2021). Microtubules and the plus-end binding protein EB1 (Bim1 in yeast) contribute to endocytosis in *Drosophila melanogaster* oocytes, although roles for clathrin in this process have not been addressed (Sanghavi *et al.*, 2012). Lastly, RhoA and integrins (similar to yeast Rho1 and Mid2, respectively) are required for clathrin-independent compensatory endocytosis in bladder umbrella cells and for internalization of the IL-2 receptor (Lamaze *et al.*, 2001; Khandelwal *et al.*, 2010). While additional parallels likely exist, these suggest that the protein machinery involved in a variety of CIE pathways may at least partially overlap. Alternatively, yeast CIE may represent an ancestral form of clathrin-independent endocytosis that has branched or diverged during evolution. It will be interesting to test whether additional components of the yeast pathway contribute to CIE mechanisms in other eukaryotes, and our ability to identify additional CIE components using yeast genetics has the potential to rapidly expand our understanding of these pathways.

With an increase in our understanding of CIE pathways and the protein machinery that enables clathrin-independent internalization, insights into relationships between CIE and human diseases may also emerge. To date, homologues of several yeast CIE proteins have been linked to disease. For example, mutations in diaphanous-related formins, which are homologous to yeast Bni1, are associated with microcephaly and related developmental disorders (Labat-de-Hoz and Alonso, 2021). From our current study, Pac1 is related to the lissencephaly related protein LIS1, while Kar9 is related to the APC protein involved in colorectal cancer (Geiser *et al.*, 1997; Korinek *et al.*, 2000). Moreover, the dynactin p150[Glued] subunit associates with the huntingtin-associated protein HAP1 (Li *et al.*, 1998); these may act in a complex involved in vesicular transport, particularly in axons. While direct roles for these proteins in mammalian CIE remain unclear, both in health and disease, it will be interesting to assess whether disease-linked mutations or losses of function alter cargo internalization, and whether such an effect might contribute to cellular dysfunction in disease.

Overall, our findings lead us to propose a model in which the interplay between myosin- and actin-dependent transport of microtubules, their cortical capture, and activation of dynein/dynactin promote CIE in yeast (Figure 8). While individual proteins within these modules may have more or less prominent roles, as seen by differences in the magnitude of change in our quantitative analyses using Ste3-pHluorin, each of the modules nonetheless appears to contribute to CIE, likely through a series of related events. For example, Myo2-dependent delivery of microtubule plus ends to the cell cortex requires Kar9 and Bim1. As the plus end is transported through the cytoplasm, tracking proteins such as Bik1 and Pac1 promote loading and retention of dynein/dynactin, albeit in an inhibited state, and redundant pathways involving these proteins help to ensure the fidelity of microtubule delivery to the cell cortex (Miller and Rose, 1998; Adames and Cooper, 2000; Lee *et al.*, 2000; Miller *et al.*, 2000; Yin *et al.*, 2000; Farkasovsky and Küntzel, 2001). Once delivered to the cell periphery, a hand-off event occurs wherein dynein associates with the cMT-capturing protein Num1, leading to cMT offloading from Myo2, dynein activation and minus-end directed motility (Lee *et al.*, 2003, 2005). These events are thought to be necessary for the force generation required to position the nucleus at the bud neck during mitosis, thereby ensuring chromosome segregation and nuclear partitioning between mother and daughter cells. However, because dynein is tethered to Num1 at the cell cortex during this process, it seems plausible that minus-end directed motor activity could also exert inward force at the PM. Combined with Bni1-generated actin filaments and Myo2 motor activity, this could facilitate membrane bending in the absence of clathrin, which is needed to overcome the high turgor pressure in yeast cells (Aghamohammadzadeh and Ayscough, 2009). Alternatively, PM force generation might activate Mid2 signaling, leading to a localized increase in Rho1 function. Our observation that cytoplasmic microtubules contribute to the Rho1 pathway supports a role in CIE, even though they appear to be sparse under most conditions in budding yeast. It is thus plausible that microtubule cytoskeleton-stabilizing environmental conditions could provide clues about how yeast CIE is regulated. Our future studies will examine this possibility, and will further test roles for the interaction network between actin, microtubules, and their respective motor proteins in membrane and cargo internalization.

MATERIALS AND METHODS
Request a protocol through Bio-protocol.

Yeast strains, plasmids, and growth conditions
Strains and plasmids used in this study are described in Supplemental Tables S1 and S2, respectively. Yeast were grown in liquid or plate-based YPD medium or on YNB (synthetic defined) medium lacking uracil, tryptophan, histidine and/or lysine for maintenance of nonessential plasmids. All cells were grown at 30°C and imaged at room temperature. PCR-based tagging of genomic loci and gene knockouts were performed as described previously (Longtine *et al.*, 1998; Goldstein and McCusker, 1999). Transformations for plasmid uptake or for genomic integrations were performed using the LiAc method (Schiestl and Gietz, 1989). Unless otherwise specified, chemicals and reagents were purchased from Sigma-Aldrich or from Thermo Fisher Scientific.

Construction and confirmation of MYO2 IQ repeat truncations
Plasmids for truncating Myo2 IQ repeats at the genomic *MYO2* locus with *HIS3* selection were generously provided by Dr. Anthony Bretscher (Cornell; Schott *et al.*, 1999, 2002). The full-length control *MYO2[6IQ]* plasmid was linearized with SpeI, while the truncated *myo2[4IQ]* and *myo2[2IQ]* plasmids were linearized with BamHI, transformed into SEY6210 *MATα* WT or *ent1::LEU2 yap1802::LEU2*

cells, and selected on YNB medium lacking histidine. *ent1::LEU2 yap1802::LEU2* cells with Myo2 modifications were then mated with *MATa ent2::HIS3 yap1801::HIS3* cells. Resulting diploids were transformed with pENT2.416 [*CEN URA3*], sporulated and tetrad dissected, and resulting *ent1::LEU2 ent2::HIS3 yap1801::HIS3 yap1802::LEU2*+pENT2.416 (4Δ+Ent2) cells were confirmed by PCR. Cells were then transformed with pENT1.414 or pENTH1.414 and grown on 5-FOA plates to select for loss of the pENT2.416 plasmid, yielding 4Δ+Ent1 and 4Δ+ENTH1 cells with WT or truncated Myo2. All Myo2 truncations were confirmed by PCR using the following primers: 5'-TTGATGGTGTTGTCTCAACTCAGAG-3' and 5'-CATT-GATTTGTGTAGCATTGACACC-3', which amplify nucleotides 2047-3472 of the WT *MYO2* coding sequence containing the IQ repeat region. PCR products were then resolved by gel electrophoresis, and truncations were confirmed by differences in size compared with full-length *MYO2*.

Construction and confirmation of myo2 CBD mutant strains

Plasmids for low-copy expression of *MYO2* or *myo2^CBD* mutants with *HIS3* selection were generous gifts from Dr. Lois Weisman (Univ. Michigan; Catlett and Weisman, 1998; Ishikawa *et al.*, 2003; Pashkova *et al.*, 2006; Eves *et al.*, 2012). We used these as a starting point for generating chromosomally integrated CBD mutants at the endogenous *MYO2* locus and expressed as the sole source of Myo2. To accomplish this, we isolated the 1.5 kb EcoRI fragment from WT and CBD mutant Myo2.413 plasmids containing the C-terminal CBD and 3' untranslated region of *MYO2* for subcloning into the EcoRI site of pRS404. Resulting plasmids were confirmed by sequencing, and the orientation of all inserts placed the 5' end of the Myo2 CBD proximal to the KpnI end of the polylinker. The plasmids were then linearized with NruI, transformed into SEY6210 *MATα* WT or 4Δ+pENT2.416 cells, and selected on YNB medium lacking tryptophan. 4Δ+Ent2 cells were then transformed with pENT1.317 or pENTH1.317 and selected on YNB medium lacking lysine. Cells were subsequently grown on 5-FOA plates to select for loss of the pENT2.416 plasmid, yielding Myo2 WT or CBD mutant-expressing 4Δ+Ent1 and 4Δ+ENTH1 strains. All WT and 4Δ strains with Myo2 CBD modifications were confirmed by isolation of genomic DNA and PCR amplification of the *MYO2* CBD using forward primer 5'-CTACCTCAAACACCATTAAAGGATG-3' and T3 as the reverse primer. The resulting 1683 bp product spanning the 3' end of *MYO2* upstream of the integration site through the 3' untranslated region was then isolated using a PCR purification kit (Qiagen), and mutations were confirmed by sequencing using primer 5'-CT-CATTTGTGGTGTTTGCTC-3', which anneals to the *MYO2* CDS beginning at nucleotide 3777 downstream of the +1 site.

LatA and Nocodazole treatment

Liquid cultures of WT, 4Δ+Ent1 and 4Δ+ENTH1 cells expressing Ste3-GFP and transformed with empty vector (pRS426) or high-copy *ROM1* were grown to mid-logarithmic phase at 30°C in YNB medium lacking uracil (Christianson *et al.*, 1992; Ozaki *et al.*, 1996). A total of 0.7 OD_{600} of each strain was then pelleted by centrifugation at 3500 × g for 5 min, and cells were resuspended in 25 µl of YNB -ura medium supplemented with 200 µM LatA (Enzo Life Sciences), 15 µg/ml Nocodazole, or an equivalent volume of DMSO as a vehicle control. Cells were then incubated at 30°C for 2 h before imaging by fluorescence microscopy.

Visualization of actin morphology

To visualize actin patches and cables, yeast cells were stained using a protocol modified from (Amberg, 1998). Briefly, *myo3Δ myo5Δ*

cells were grown to mid-logarithmic phase in YNB medium lacking uracil for plasmid selection. Cells were fixed at room temperature for 30 min by addition of formaldehyde to a final concentration of 4% (vol/vol), then pelleted by centrifugation at 3000 × g for 5 min. Pellets were washed twice with phosphate-buffered saline (PBS) and stained for 1 h with Alexa 568 phalloidin (Thermo Fisher) dissolved in methanol, and diluted to a final concentration of 1.65 µM in PBS. Cells were then washed three times with PBS before imaging by fluorescence microscopy.

Fluorescence microscopy and image analysis

Images were collected using either an Axiovert 200 inverted fluorescence microscope (Zeiss) equipped with a 100X, 1.4 NA Plan-Apochromat oil-immersion objective, Sensicam (Cooke), X-Cite 120 PC light source, and SlideBook 4.2 software (3i) or using a DMi8 inverted fluorescence microscope (Leica) equipped with a 100X, 1.47 NA Plan-Apochromat oil-immersion objective, LED3 fluorescence illumination system, Flash 4.0 v3 sCMOS camera (Hamamatsu) and LAS X v3.7.6.25997 (Leica). Within each experiment, all strains were imaged with the same acquisition parameters and on the same day. All imaging was performed using cells grown to mid-logarithmic phase.

Following acquisition, images were processed using Fiji/ImageJ2 v2.9.0/1.53t. Within each experiment, identical post-imaging processing was performed on all images to set identical minimum- and maximum-intensity levels, allowing direct comparison of protein localization and fluorescence intensity.

For visualization of phalloidin-labeled cells, z-stacks were collected at 0.25 µm step intervals spanning the entire depth of cells. Stacks were then collapsed into a maximum-intensity z-projection image using Fiji/ImageJ2.

Quantification of Ste3-pHluorin intensity

Quantification of Ste3-pHluorin intensity was performed as described previously (Prosser *et al.*, 2010, 2016). Briefly, random fields of cells for each condition analyzed were visualized by DIC before imaging by fluorescence microscopy. All conditions within an experiment (e.g., WT + vector, 4Δ+Ent1 + vector, 4Δ+ENTH1 + vector, and 4Δ+ENTH1 + *ROM1*) were imaged on the same day, using identical acquisition parameters to allow direct comparison of groups within that experiment. Complete experiments were collected using one of two microscopes as noted above (Leica DMi8 for Figures 1, 2, and 4; Axiovert 200 for Figures 3, 5, 6, and 7), which each gave different y-axis scales for fluorescence intensity based on the microscope used; however, we verified that relative/fold changes in pHluorin intensity remained similar in control experiments regardless of the difference in y-axis scale (Figures 1B, 2B, 3B, 4B, and unpublished data). In preparing figures, we used matched y-axis scaling for all quantitative analyses from each of the two microscopes (maximum value of 4000 for all results collected on the Leica DMi8 microscope, and 350 for all results collected on the Axiovert 200 microscope). For all quantitative experiments, background subtraction was then performed on 16-bit images, individual cells were selected for measurement of whole-cell fluorescence intensity, and values were corrected for cell size. Predetermined criteria for exclusion of cells from analysis are described in (Prosser *et al.*, 2016).

Statistical analysis

Power analysis was performed to determine population sizes using G*Power v3.1.9.6, with type I error α = 0.05, type II error β = 0.2 (power, 1-β = 0.8), and a moderate effect size f = 0.3. For experiments with four groups (WT, 4Δ+Ent1 and 4Δ+ENTH1 backgrounds

with empty vector; 4Δ+ENTH1 with high-copy *ROM1*) using one-way ANOVA, the analysis recommended a minimum of 32 cells measured per condition.

Statistical significance for all quantitative experiments was assessed using one-way ANOVA followed by Tukey's Multiple Comparison test in Prism 7 (GraphPad).

ACKNOWLEDGMENTS

REFERENCES

Adames NR, Cooper JA (2000). Microtubule interactions with the cell cortex causing nuclear movements in *Saccharomyces cerevisiae*. J Cell Biol 149, 863–874.

Aghamohammadzadeh S, Ayscough KR (2009). Differential requirements for actin during yeast and mammalian endocytosis. Nat Cell Biol 11, 1039–1042.

Aguilar RC, Longhi SA, Shaw JD, Yeh L-Y, Kim S, Schön A, Freire E, Hsu A, McCormick WK, Watson HA, Wendland B (2006). Epsin N-terminal homology domains perform an essential function regulating Cdc42 through binding Cdc42 GTPase-activating proteins. Proc Natl Acad Sci USA 103, 4116–4121.

Amberg DC (1998). Three-dimensional imaging of the yeast actin cytoskeleton through the budding cell cycle. Mol Biol Cell 9, 3259–3262.

Anderson E, Batten BE (1983). Surface binding, uptake and fate of cationic ferritin in a steroid producing ovarian cell. Tissue Cell 15, 853–871.

Anderson BL, Boldogh I, Evangelista M, Boone C, Greene LA, Pon LA (1998). The Src homology domain 3 (SH3) of a yeast type I myosin, Myo5p, binds to verprolin and is required for targeting to sites of actin polarization. J Cell Biol 141, 1357–1370.

Anderson HL, Casler JC, Lackner LL (2022). Hierarchical integration of mitochondrial and nuclear positioning pathways by the Num1 EF hand. Mol Biol Cell 33, ar20.

Apel AR, Hoban K, Chuartzman S, Tonikian R, Sidhu S, Schuldiner M, Wendland B, Prosser D (2017). Syp1 regulates the clathrin-mediated and clathrin-independent endocytosis of multiple cargo proteins through a novel sorting motif. Mol Biol Cell 28, 2434–2448.

Barker SL, Lee L, Pierce BD, Maldonado-Báez L, Drubin DG, Wendland B (2007). Interaction of the endocytic scaffold protein Pan1 with the type I myosins contributes to the late stages of endocytosis. Mol Biol Cell 18, 2893–2903.

Beach DL, Thibodeaux J, Maddox P, Yeh E, Bloom K (2000). The role of the proteins Kar9 and Myo2 in orienting the mitotic spindle of budding yeast. Curr Biol 10, 1497–1506.

van der Bliek A, Redelmeier T, Damke H, Tisdale E, Meyerowitz E, Schmid S (1993). Mutations in human dynamin block an intermediate stage in coated vesicle formation. J Cell Biol 122, 553–563.

Bobola N, Jansen R-P, Shin TH, Nasmyth K (1996). Asymmetric accumulation of Ash1p in postanaphase nuclei depends on a myosin and restricts yeast mating-type switching to mother cells. Cell 84, 699–709.

Boldogh IR, Ramcharan SL, Yang H-C, Pon LA (2004). A type V myosin (Myo2p) and a Rab-like G-Protein (Ypt11p) are required for retention of newly inherited mitochondria in yeast cells during cell division. Mol Biol Cell 15, 3994–4002.

Boscheron C, Caudron F, Loeillet S, Peloso C, Mugnier M, Kurzawa L, Nicolas A, Denarier E, Aubry L, Andrieux A (2016). A role for the yeast CLIP170 ortholog, the plus-end-tracking protein Bik1, and the Rho1 GTPase in Snc1 trafficking. J Cell Sci 129, 3332–3341.

Boucrot E, Ferreira APA, Almeida-Souza L, Debard S, Vallis Y, Howard G, Bertot L, Sauvonnet N, McMahon HT (2015). Endophilin marks and controls a clathrin-independent endocytic pathway. Nature 517, 460–465.

Burke TA, Christensen JR, Barone E, Suarez C, Sirotkin V, Kovar DR (2014). Homeostatic actin cytoskeleton networks are regulated by assembly factor competition for monomers. Curr Biol 24, 579–585.

Casamento A, Boucrot E (2020). Molecular mechanism of Fast Endophilin-Mediated Endocytosis. Biochem J 477, 2327–2345.

Catlett NL, Weisman LS (1998). The terminal tail region of a yeast myosin-V mediates its attachment to vacuole membranes and sites of polarized growth. Proc National Acad Sci USA 95, 14799–14804.

Christianson TW, Sikorski RS, Dante M, Shero JH, Hieter P (1992). Multifunctional yeast high-copy-number shuttle vectors. Gene 110, 119–122.

Cuschieri L, Miller R, Vogel J (2006). γ-Tubulin Is required for proper recruitment and assembly of Kar9–Bim1 complexes in budding yeast. Mol Biol Cell 17, 4420–4434.

Damke H, Baba T, Warnock DE, Schmid SL (1994). Induction of mutant dynamin specifically blocks endocytic coated vesicle formation. J Cell Biol 127, 915–934.

Davis N, Horecka J, Sprague G (1993). Cis- and trans-acting functions required for endocytosis of the yeast pheromone receptors. J Cell Biol 122, 53–65.

Day CA, Baetz NW, Copeland CA, Kraft LJ, Han B, Tiwari A, Drake KR, Luca HD, Chinnapen DJ-F, Davidson MW, *et al.* (2015). Microtubule motors power plasma membrane tubulation in clathrin-independent endocytosis. Traffic 16, 572–590.

Epp E, Walther A, Lépine G, Leon Z, Mullick A, Raymond M, Wendland J, Whiteway M (2010). Forward genetics in *Candida albicans* that reveals the Arp2/3 complex is required for hyphal formation, but not endocytosis. Mol Microbiol 75, 1182–1198.

Epp E, Nazarova E, Regan H, Douglas LM, Konopka JB, Vogel J, Whiteway M (2013). Clathrin- and Arp2/3-independent endocytosis in the fungal pathogen *Candida albicans*. MBio 4, e00476–13.

Eshel D, Urrestarazu LA, Vissers S, Jauniaux JC, Vliet-Reedijk JC, Planta RJ, Gibbons IR (1993). Cytoplasmic dynein is required for normal nuclear segregation in yeast. Proc National Acad Sci USA 90, 11172–11176.

Evangelista M, Pruyne D, Amberg DC, Boone C, Bretscher A (2001). Formins direct Arp2/3-independent actin filament assembly to polarize cell growth in yeast. Nat Cell Biol 4, 32–41.

Eves PT, Jin Y, Brunner M, Weisman LS (2012). Overlap of cargo binding sites on myosin V coordinates the inheritance of diverse cargoes. J Cell Biol 198, 69–85.

Fagarasanu M, Fagarasanu A, Tam YYC, Aitchison JD, Rachubinski RA (2005). Inp1p is a peroxisomal membrane protein required for peroxisome inheritance in *Saccharomyces cerevisiae*. J Cell Biol 169, 765–775.

Fagarasanu A, Mast FD, Knoblach B, Jin Y, Brunner MJ, Logan MR, Glover JNM, Eitzen GA, Aitchison JD, Weisman LS, Rachubinski RA (2009). Myosin-driven peroxisome partitioning in *S. cerevisiae*. J Cell Biol 186, 541–554.

Farkasovsky M, Küntzel H (1995). Yeast Num1p associates with the mother cell cortex during S/G2 phase and affects microtubular functions. J Cell Biol 131, 1003–1014.

Farkasovsky M, Küntzel H (2001). Cortical Num1p interacts with the dynein intermediate chain Pac11p and cytoplasmic microtubules in budding yeast. J Cell Biol 152, 251–262.

Farrell KB, McDonald S, Lamb AK, Worcester C, Peersen OB, Pietro SMD (2017). Novel function of a dynein light chain in actin assembly during clathrin-mediated endocytosis. J Cell Biol 216, 2565–2580.

Ferreira APA, Casamento A, Roas SC, Halff EF, Panambalana J, Subramaniam S, Schützenhofer K, Hak LCW, McGourty K, Thalassinos K, *et al.* (2021). Cdk5 and GSK3β inhibit fast endophilin-mediated endocytosis. Nat Commun 12, 2424.

Gachet Y, Hyams JS (2005). Endocytosis in fission yeast is spatially associated with the actin cytoskeleton during polarised cell growth and cytokinesis. J Cell Sci 118, 4231–4242.

Geiser JR, Schott EJ, Kingsbury TJ, Cole NB, Totis LJ, Bhattacharyya G, He L, Hoyt MA (1997). Saccharomyces cerevisiae genes required in the absence of the CIN8-encoded spindle motor act in functionally diverse mitotic pathways. Mol Biol Cell 8, 1035–1050.

Geli MI, Riezman H (1996). Role of type I myosins in receptor-mediated endocytosis in yeast. Science 272, 533–535.

Goldstein AL, McCusker JH (1999). Three new dominant drug resistance cassettes for gene disruption in *Saccharomyces cerevisiae*. Yeast 15, 1541–1553.

Goode BL, Eskin JA, Wendland B (2015). Actin and Endocytosis in Budding Yeast. Genetics 199, 315–358.

Goodson HV, Anderson BL, Warrick HM, Pon LA, Spudich JA (1996). Synthetic lethality screen identifies a novel yeast myosin I gene (*MYO5*): myosin I proteins are required for polarization of the actin cytoskeleton. J Cell Biol 133, 1277–1291.

Howard JP, Hutton JL, Olson JM, Payne GS (2002). Sla1p serves as the targeting signal recognition factor for NPFX(1,2)D-mediated endocytosis. J Cell Biol 157, 315–326.

Howes MT, Kirkham M, Riches J, Cortese K, Walser PJ, Simpson F, Hill MM, Jones A, Lundmark R, Lindsay MR, *et al.* (2010). Clathrin-independent carriers form a high capacity endocytic sorting system at the leading edge of migrating cells. J Cell Biol 190, 675–691.

Ishikawa K, Catlett NL, Novak JL, Tang F, Nau JJ, Weisman LS (2003). Identification of an organelle-specific myosin V receptor. J Cell Biol 160, 887–897.

Jin Y, Sultana A, Gandhi P, Franklin E, Hamamoto S, Khan AR, Munson M, Schekman R, Weisman LS (2011). Myosin V transports secretory vesicles via a Rab GTPase cascade and interaction with the exocyst complex. Dev Cell 21, 1156–1170.

Johnston GC, Prendergast JA, Singer RA (1991). The *Saccharomyces cerevisiae MYO2* gene encodes an essential myosin for vectorial transport of vesicles. J Cell Biol 113, 539–551.

Kahana JA, Schlenstedt G, Evanchuk DM, Geiser JR, Hoyt MA, Silver PA (1998). The yeast dynactin complex is involved in partitioning the mitotic spindle between mother and daughter cells during anaphase B. Mol Biol Cell 9, 1741–1756.

Kaksonen M, Roux A (2018). Mechanisms of clathrin-mediated endocytosis. Nat Rev Mol Cell Bio 19, 313–326.

Kaksonen M, Sun Y, Drubin DG (2003). A pathway for association of receptors, adaptors, and actin during endocytic internalization. Cell 115, 475–487.

Kaksonen M, Toret CP, Drubin DG (2005). A modular design for the clathrin- and actin-mediated endocytosis machinery. Cell 123, 305–320.

Kanaseki T, Kadota K (1969). The "Vesicle in a Basket." J Cell Biol 42, 202–220.

Khandelwal P, Ruiz WG, Apodaca G (2010). Compensatory endocytosis in bladder umbrella cells occurs through an integrin-regulated and RhoA- and dynamin-dependent pathway. EMBO J 29, 1961–1975.

Korinek WS, Copeland MJ, Chaudhuri A, Chant J (2000). Molecular linkage underlying microtubule orientation toward cortical sites in yeast. Science 287, 2257–2259.

Labat-de-Hoz L, Alonso MA (2021). Formins in Human Disease. Cells 10, 2554.

Lamaze C, Dujeancourt A, Baba T, Lo CG, Benmerah A, Dautry-Varsat A (2001). Interleukin 2 receptors and detergent-resistant membrane domains define a clathrin-independent endocytic pathway. Mol Cell 7, 661–671.

Lee L, Tirnauer JS, Li J, Schuyler SC, Liu JY, Pellman D (2000). Positioning of the mitotic spindle by a cortical-microtubule capture mechanism. Science 287, 2260–2262.

Lee W-L, Oberle JR, Cooper JA (2003). The role of the lissencephaly protein Pac1 during nuclear migration in budding yeast. J Cell Biol 160, 355–364.

Lee W-L, Kaiser MA, Cooper JA (2005). The offloading model for dynein function. J Cell Biol 168, 201–207.

Lee YJ, Shi R, Witt SN (2013). The small molecule triclabendazole decreases the intracellular level of cyclic AMP and increases resistance to stress in *Saccharomyces cerevisiae*. PLoS ONE 8, e64337.

Lewis MJ, Nichols BJ, Prescianotto-Baschong C, Riezman H, Pelham HR (2000). Specific retrieval of the exocytic SNARE Snc1p from early yeast endosomes. Mol Biol Cell 11, 23–38.

Li S-H, Gutekunst C-A, Hersch SM, Li X-J (1998). Interaction of huntingtin-associated protein with dynactin P150Glued. J Neurosci 18, 1261–1269.

Lipatova Z, Tokarev AA, Jin Y, Mulholland J, Weisman LS, Segev N (2008). Direct interaction between a myosin V motor and the Rab GTPases Ypt31/32 is required for polarized secretion. Mol Biol Cell 19, 4177–4187.

Longtine MS, Demarini AM III, Shah DJ, Wach NG, Brachat A, Philippsen P, Pringle JR (1998). Additional modules for versatile and economical PCR-based gene deletion and modification in *Saccharomyces cerevisiae*. Yeast 14, 953–961.

Maldonado-Báez L, Dores MR, Perkins EM, Drivas TG, Hicke L, Wendland B (2008). Interaction between Epsin/Yap180 adaptors and the scaffolds Ede1/Pan1 is required for endocytosis. Mol Biol Cell 19, 2936–2948.

Mayor S, Parton RG, Donaldson JG (2014). Clathrin-independent pathways of endocytosis. Cold Spring Harb Perspect Biol 6, a016758.

Miesenböck G, Angelis DAD, Rothman JE (1998). Visualizing secretion and synaptic transmission with pH-sensitive green fluorescent proteins. Nature 394, 192–195.

Miller RK, Heller KK, Frisèn L, Wallack DL, Loayza D, Gammie AE, Rose MD (1998). The kinesin-related proteins, Kip2p and Kip3p, function differently in nuclear migration in yeast. Mol Biol Cell 9, 2051–2068.

Miller RK, Cheng SC, Rose MD (2000). Bim1p/Yeb1p mediates the Kar9p-dependent cortical attachment of cytoplasmic microtubules. Mol Biol Cell 11, 2949–2959.

Miller RK, Rose MD (1998). Kar9p Is a novel cortical protein required for cytoplasmic microtubule orientation in yeast. J Cell Biol 140, 377–390.

Moore JK, D'Silva S, Miller RK (2006). The CLIP-170 Homologue Bik1p Promotes the Phosphorylation and Asymmetric Localization of Kar9p. Mol Biol Cell 17, 178–191.

Morris RE, Saelinger CB (1983). Diphtheria toxin does not enter resistant cells by receptor-mediated endocytosis. Infect Immun 42, 812–817.

Newpher TM, Smith RP, Lemmon V, Lemmon SK (2005). In vivo dynamics of clathrin and its adaptor-dependent recruitment to the actin-based endocytic machinery in yeast. Dev Cell 9, 87–98.

Ozaki K, Tanaka K, Imamura H, Hihara T, Kameyama T, Nonaka H, Hirano H, Matsuura Y, Takai Y (1996). Rom1p and Rom2p are GDP/GTP exchange proteins (GEPs) for the Rho1p small GTP binding protein in *Saccharomyces cerevisiae*. EMBO J 15, 2196–2207.

Pashkova N, Jin Y, Ramaswamy S, Weisman LS (2006). Structural basis for myosin V discrimination between distinct cargoes. EMBO J 25, 693–700.

Pearse BMF (1975). Coated vesicles from pig brain: Purification and biochemical characterization. J Mol Biol 97, 93–98.

Prosser DC, Whitworth K, Wendland B (2010). Quantitative analysis of endocytosis with cytoplasmic pHluorin chimeras. Traffic 11, 1141–1150.

Prosser DC, Drivas TG, Maldonado-Báez L, Wendland B (2011). Existence of a novel clathrin-independent endocytic pathway in yeast that depends on Rho1 and formin. J Cell Biol 195, 657–671.

Prosser DC, Pannunzio AE, Brodsky JL, Thorner J, Wendland B, O'Donnell AF (2015). α-Arrestins participate in cargo selection for both clathrin-independent and clathrin-mediated endocytosis. J Cell Sci 128, 4220–4234.

Prosser DC, Wrasman K, Woodard TK, O'Donnell AF, Wendland B (2016). Applications of pHluorin for Quantitative, Kinetic and High-throughput Analysis of Endocytosis in Budding Yeast. J Vis Exp (116), e54587.

Prosser DC, Wendland B (2012). Conserved roles for yeast Rho1 and mammalian RhoA GTPases in clathrin-independent endocytosis. Small GTPases 3, 229–235.

Pruyne DW, Schott DH, Bretscher A (1998). Tropomyosin-containing actin cables direct the Myo2p-dependent polarized delivery of secretory vesicles in budding yeast. J Cell Biol 143, 1931–1945.

Pruyne D, Evangelista M, Yang C, Bi E, Zigmond S, Bretscher A, Boone C (2002). Role of formins in actin assembly: Nucleation and barbed-end association. Science 297, 612–615.

Pruyne D, Legesse-Miller A, Gao L, Dong Y, Bretscher A (2004). Mechanisms of polarized growth and organelle segregation in yeast. Annu Rev Cell Dev Biol 20, 559–591.

Radhakrishna H, Klausner RD, Donaldson JG (1996). Aluminum fluoride stimulates surface protrusions in cells overexpressing the ARF6 GTPase. J Cell Biol 134, 935–947.

Reider A, Barker SL, Mishra SK, Im YJ, Maldonado-Báez L, Hurley JH, Traub LM, Wendland B (2009). Syp1 is a conserved endocytic adaptor that contains domains involved in cargo selection and membrane tubulation. EMBO J 28, 3103–3116.

Reider A, Wendland B (2011). Endocytic adaptors - social networking at the plasma membrane. J Cell Sci 124, 1613–1622.

Roth TF, Porter KR (1964). Yolk protein uptake in the oocyte of the mosquito *Aedes aegypti*. J Cell Biol 20, 313–332.

Sabharanjak S, Sharma P, Parton RG, Mayor S (2002). GPI-anchored proteins are delivered to recycling endosomes via a distinct cdc42-regulated, clathrin-independent pinocytic pathway. Dev Cell 2, 411–423.

Sagot I, Klee SK, Pellman D (2002). Yeast formins regulate cell polarity by controlling the assembly of actin cables. Nat Cell Biol 4, 42–50.

Sanghavi P, Lu S, Gonsalvez GB (2012). A functional link between localized Oskar, dynamic microtubules, and endocytosis. Dev Biol 367, 66–77.

Sankaranarayanan S, Angelis DD, Rothman JE, Ryan TA (2000). The use of pHluorins for optical measurements of presynaptic activity. Biophys J 79, 2199–2208.

Schiestl RH, Gietz RD (1989). High efficiency transformation of intact yeast cells using single stranded nucleic acids as a carrier. Curr Genet 16, 339–346.

Schott D, Ho J, Pruyne D, Bretscher A (1999). The COOH-terminal domain of Myo2p, a yeast myosin V, has a direct role in secretory vesicle targeting. J Cell Biol 147, 791–808.

Schott DH, Collions RN, Bretscher A (2002). Secretory vesicle transport velocity in living cells depends on the myosin-V lever arm length. J Cell Biol 156, 35–40.

Schwartz K, Richards K, Botstein D (1997). BIM1 encodes a microtubule-binding protein in yeast. Mol Biol Cell 8, 2677–2691.

Sharma DK, Choudhury A, Singh RD, Wheatley CL, Marks DL, Pagano RE (2002). Glycosphingolipids Internalized via Caveolar-related Endocytosis Rapidly Merge with the Clathrin Pathway in Early Endosomes and Form Microdomains for Recycling. J Biol Chem 278, 7564–7572.

Sheeman B, Carvalho P, Sagot I, Geiser J, Kho D, Hoyt MA, Pellman D (2003). Determinants of *S. cerevisiae* dynein localization and activation: implications for the mechanism of spindle positioning. Curr Biol 13, 364–372.

Soykan T, Kaempf N, Sakaba T, Vollweiter D, Goerdeler F, Puchkov D, Kononenko NL, Haucke V (2017). Synaptic Vesicle Endocytosis Occurs on Multiple Timescales and Is Mediated by Formin-Dependent Actin Assembly. Neuron 93, 854–866.e4.

Stuchell-Brereton MD, Siglin A, Li J, Moore JK, Ahmed S, Williams JC, Cooper JA (2011). Functional interaction between dynein light chain and intermediate chain is required for mitotic spindle positioning. Mol Biol Cell 22, 2690–2701.

Suarez C, Carroll RT, Burke TA, Christensen JR, Bestul AJ, Sees JA, James ML, Sirotkin V, Kovar DR (2015). Profilin regulates F-actin network homeostasis by favoring formin over Arp2/3 complex. Dev Cell 32, 43–53.

Sun Y, Martin AC, Drubin DG (2006). Endocytic internalization in budding yeast requires coordinated actin nucleation and myosin motor activity. Dev Cell 11, 33–46.

Taylor MJ, Perrais D, Merrifield CJ (2011). A high precision survey of the molecular dynamics of mammalian clathrin-mediated endocytosis. PLoS Biol 9, e1000604.

Ungewickell E, Ungewickell H, Holstein SEH, Lindner R, Prasad K, Barouch W, Martini B, Greene LE, Eisenberg E (1995). Role of auxilin in uncoating clathrin-coated vesicles. Nature 378, 632–635.

Wang Y, et al. (2012). Coiled-coil networking shapes cell molecular machinery. Mol Biol Cell 23, 3911–3922.

Watanabe S, Boucrot E (2017). Fast and ultrafast endocytosis. Curr Opin Cell Biol 47, 64–71.

Watanabe S, Liu Q, Davis MW, Hollopeter G, Thomas N, Jorgensen NB, Jorgensen EM (2013a). Ultrafast endocytosis at *Caenorhabditis elegans* neuromuscular junctions. Elife 2, e00723.

Watanabe S, Rost BR, Camacho-Pérez M, Davis MW, Söhl-Kielczynski B, Rosenmund C, Jorgensen EM (2013b). Ultrafast endocytosis at mouse hippocampal synapses. Nature 504, 242–247.

Watts FZ, Shiels G, Orr E (1987). The yeast MYO1 gene encoding a myosin-like protein required for cell division. EMBO J 6, 3499–3505.

Wendland B, Steece KE, Emr SD (1999). Yeast epsins contain an essential N-terminal ENTH domain, bind clathrin and are required for endocytosis. EMBO J 18, 4383–4393.

Yin H, Pruyne D, Huffaker TC, Bretscher A (2000). Myosin V orientates the mitotic spindle in yeast. Nature 406, 1013–1015.